



Optic disc detection and segmentation using saliency mask in retinal fundus images



Nihal Zaaboub^{a,b,*}, Faten Sandid^b, Ali Douik^{b,c}, Basel Solaiman^d

^a ENIT: National Engineering School of Tunis, University Tunis El Manar, Tunisia

^b NOCCS-ENISO: Networked Objects Control and Communication Systems Laboratory, Tunisia

^c ENISO: National Engineering School of Sousse, University of Sousse, Tunisia

^d Image & Information Processing Department (ITI), IMT-Atlantique, Technopôle Brest Iroise CS 83818, 29238 Brest, France

ARTICLE INFO

Keywords:

Optic disc
Object localization and segmentation
Saliency mask
Retinal fundus image

ABSTRACT

Background and objective: Detection of the Optic Disc (OD) in retinal fundus image is crucial in identifying diverse abnormal conditions in the retina such as diabetic retinopathy. Previous systems are oriented to the OD detection and segmentation. Most research failed to locate the OD in the case when the image does not have a criterion appearance. The objective of the proposed work is to precisely define a new and robust OD segmentation in color retinal fundus images.

Methods: The proposed algorithm is composed of two stages: OD localization and segmentation. The first phase consists in the OD localization through: 1) a preprocessing step; 2) vessel extraction and elimination, and 3) a geometric analysis allowing to decide the OD location. For the second phase, a set of is computed in order to produce various candidates. A combination of these candidates accurately forms a completed contour of the OD.

Results: The proposed method is evaluated using 10 publicly available databases as well as a local database. Accuracy rates in the RimOne and IDRID databases are 98.06% and 99.71%, respectively, and 100% for the Chase, Drive, HRF, Drishti, Drions, Bin Rushed, Magrabiya, Messidor and LocaliDB databases with an overall success rate of 99.80% and specificity rates of 99.44%, 99.64%, 99.66%, 99.66%, 99.70%, 99.87%, 99.72%, 99.83% and 99.82% for the Rim One, Drions, IDRID, Drishti, HRF, Bin Rushed, Magrabiya, Messidor and proprietary databases.

Conclusion: The main advantage of the proposed approach is the robustness and the excellent performances even with critical cases of retinal images. The proposed method achieves the state-of-the-art performances with regards to the OD detection and segmentation. It is also of a great interest for clinical usage without the expert intervention to treat each image.

1. Introduction

Based on statistics from the World Health Organization (WHO) [1], glaucoma and Diabetic Retinopathy (DR) are the most dangerous anomalies since they are the major causes of blindness in the world [2]. This type of disease precisely affects the retina [3] and it is manually diagnosed by ophthalmologists. The main challenge in diagnosing DR is that it does not have symptoms in the early stages [2], hence, there is a huge need for regular and periodic analysis. According to world statistics, half of people who suffering from glaucoma don't know that they have the disease.

In fact, glaucoma is a progressive optic-nerve lesion easily visible

only on fundus images. The best way to screen for glaucoma is to identify the early optic-nerve signs, as well as the Optic Disc (OD) damage. Therefore, a very important step before the diagnosis of this kind of diseases is the OD localization and segmentation. To do so, physicians have to manually draw the boundaries of the OD and the Optic Cup (OC) to calculate the cup-to-disc ratio. On the other hand, manual analysis takes a lot of manpower, time, cost and labor and, thus, unrealistic for a large population [4]. Note that, in a color fundus image, the main retinal image features are the OD, the OC, the vascular system, the fovea and the macula. The most important feature in fundus images is the OD is important, besides the fovea and the vascular system. The OD appearance is similar to other types of anomalies like the exudate. Therefore,

* Corresponding author. ENIT: National Engineering School of Tunis, University Tunis El Manar, Tunisia.

E-mail addresses: nihel.zaaboub@enit.utm.tn, nihelzaaboub@gmail.com (N. Zaaboub).

the OD segmentation becomes an essential step recommended before several processing such as: the segmentation of the exudate [5,6], the localization of the fovea or macula [7], the diagnosis of glaucoma, the classification of left and right eyes in the fundus retinal images or the laser application. The last one is a treatment used to reduce the propagation of DR. Before applying this treatment step, ophthalmologists have to determine the precise boundary of the retinal structure such as the OD to avoid the laser application on this region.

The literature survey shows that there are many pieces of work on optic disc localization and segmentation in fundus retinal colored images [8]. In the literature, it can be noticed the existence of three groups of OD segmentation methods [9]: the blood vessel convergence, the OD appearance-based algorithms and the model-based algorithms. First, the blood vessel convergence is used due to the fact that the convergence point of the major vascular tree is the optic disc. Therefore, the employment of the blood vessels information is considered to locate and segment the optic disc [10,11]. Second, the OD appearance-based algorithms depend mainly on extracting the OD boundary through capturing bright and circular region. The brightness of the OD was determined using the edge detector [12], morphological operation [7, 13,14] and thresholding approaches [13]. Whereas the circularity of the object was mainly extracted using the Circular Hough Transform (CHT) [13,15,16]. Third, the model-based algorithms group includes the iterative-based algorithms such as active contour [17] and the supervised learning-based algorithms [16,18,19].

The state of art methods presents many drawbacks. In fact, the algorithms based on the OD appearance, like the size and the shape are prone to detecting false regions such as the exudates or the blood vessels instead of detecting the OD. Similar problems appear in approaches using these methods in the preprocessing step. Furthermore, the Deep Learning methods need high-end computing resources and an important large training time, which are impractical in several clinical applications. These two drawbacks limit the use of these algorithms in real-time diagnosis.

Many challenges have to be tackled in order to have a performing and accurate optic disc localization and segmentation in color fundus retinal images. First, the vessels inside the OD will make their outlines incomplete. Second, the OD area is small compared with the entire image. Third, the fundus-image characteristics vary according to the type of disease (glaucoma, neovascularization, DR, macular edema, malaria ...). Fourth, from one patient to another there is a difference in terms of shape, color, and size of OD, making, thus, the detection task more difficult. Fifth, the OD is similar in shape and size with many types of diseases such as the exudate and the wool cotton spots, which may lead to false detection. Finally, from one image acquisition device to another, there is a difference in terms of the angle of the field of view, the contrast, the brightness, the zoom, and the level of presence of artifacts in the image, which make the segmentation task even more challenging.

1.1. Contributions of the proposed method

In this paper, a new algorithm of optic disc localization and segmentation is proposed.

More specifically, the proposed algorithm uses the haze removal method allowing to enhance the contrast, which has not previously been used in the field of retinal image processing for optic disc detection. In addition, a new combination of a simple methods such as the contrast limited adaptive histogram equalization, the morphological operations and the Bernsen thresholding are used to extract the vessels. Besides, a combination of two color channels is utilized for inpainting the vessels. Furthermore, in the proposed algorithm we propose to create a saliency mask which is composed by three steps.: the supremum of opening, the image reconstruction, and the regional maxima. This new combination of known methods allows promising performances in order to detect and segment the optic disc.

In this paper, a new algorithm of OD localization and segmentation is proposed. Specifically, the main contributions discussed in this work are as follows:

- The overall accuracy in the OD detection phase is equal to 99.8% using 10 public databases as well as a local database, in a small computation time, to form 2,050 images with diverse resolutions, levels of contrast and luminosity, angles of Field of Vision (FOV), and positions of acquired images;
- The segmentation of the located OD achieves 99.63% of overall accuracy and 99.7% of specificity for all databases, which represent high performance compared to the existing approaches;
- A large number of images (2,050 images) are analyzed by our unsupervised algorithms with high accuracy. In fact, the proposed algorithm does not use the aid of any label;
- The proposed method does not require a performing processor to be used, making, thus, the proposed method applicable even with basic tools in urban zones (where the financial resources are limited). On the contrary, recent Deep Learning methods need a big amount of information for effective operations. Moreover, they are more complex than traditional methods;
- Our proposed approach is reliable with large amounts of data issued from small and diverse databases;
- The information from two relevant color channels (red and green) in the RGB color space of retinal images is used in order to avoid information loss due to channel saturation issues of other single-channel approaches, unlike the other researchers who have opted for one color channel, mostly green;
- We use a performant preprocessing step to enhance the appearance of retinal image features which has not been used for OD localization and segmentation in the literature, up to our knowledge;
- The novelty of the proposed method lies in the saliency mask creation combined by a geometric analysis. In fact, the saliency mask is based on the supremum of opening, the image reconstruction, and the regional maxima methods to locate and segment the optic disc.

In this paper, the remaining sections are organized as follows: First, we provide in section 2 a comprehensive review of the state of the art of the OD localization and segmentation methods for retinal fundus images. Second, we present in section 3 a detailed explanation of the proposed OD detection and segmentation methods. Third, a description of the evaluation metrics with the used databases is presented in section 4. Forth, section 5 represents the obtained results for both methods compared to the state-of-the-art approaches. Finally, section 6 includes concluding remarks and some future work.

2. Related works

Over the past ten years, several models have been proposed to solve a variety of challenges (detection, segmentation, and classification) on different domains (administration [20,21], satellite imagery [22], medicine [23–31], etc.). Various approaches have been presented in the literature to segment the OD boundary in retinal fundus images [8]. Different types of retinal images are used to detect the OD such as optical coherence tomography images [32], fluorescein angiography images [33] and color fundus images [34]. In fact, the optic nerve lesions such as the glaucoma can be easily observed and treated in color fundus image. In the literature, there have been several algorithms proposed for detecting and segmenting the OD in retinal fundus images.

It can be noticed that most of the algorithms, in the literature, use only one channel among the three channels of the RGB color space (Red, Green Blue) such as in Ref. [34]. Other researchers prefer converting the color fundus image to HSL (Hue, Saturation, and Lightness) color space to use the lightness channel or to convert to HSV (Hue Saturation Value) color space in order to utilize the Value channel [35,36].

As mentioned in Refs. [18,37], the methods used to segment the

optic disc in the literature can be categorized in two groups: unsupervised and supervised algorithms. Shanthi et al., [37] proposed to divide the optic disc segmentation methods into categories: edge detection methods, threshold-based methods, region-based methods, template-based methods, clustering techniques, pattern recognition techniques, and deep learning techniques.

The edge detection methods for fundus image segmentation were used in order to identify each point in the fundus image as a background or a foreground [38]. Ali et al. [39] utilized the Hough transform to locate the optic disc region and determine both the center and the diameter. A blood vessel masking step through a value close to the surrounding pixel values is used before the optic disc segmentation.

In addition, Reza et al. [38] presented a novel circle operator which based on OD properties such as the gradient property without masking the background and the vascular structure. The developed circle operator was oriented with a particular angle and pixel length depending on the OD radius. The edge detection methods use several operators in order to determine and separate the different object in the retinal fundus image. However, there is no single operator suitable with all the images. Another drawback of the edge detection method is the possibility to produce a discontinuous edge.

Concerning the threshold-based methods, they can convert a multilevel color fundus image into a binary image by choosing an appropriate threshold able to devise the fundus images into a few regions. There are two types of threshold-based methods: single [36] and adaptive [13,35]. The most used thresholding techniques are the edge maximization method, mean method and the histogram dependent method. The CHT was applied by Zahoor et al. [13] to localize and segment the OD. In fact, the authors calculated the region of interest, applied the polar transform, and used a successive morphological operation followed by an adaptive thresholding. Finally, an ellipse fitting was applied to give the precise OD boundary. The morphological operation is used by Shanthamalar et al. [14] to remove the optic disc region in which two disk structuring elements are utilized. In the approach presented by Khan et al. [35] a Dehazing method was used to enhance the fundus images followed by OD region cropping by morphological operations. Then, the vessel was detected and removed in the V channel of the HSV color space using a multi-scale line detector and a Laplace transform. After that, a local adaptive thresholding algorithm, specifically the Otsu's method, and the Region Growing (RG) are utilized to segment the OD region. A major approach disadvantage was the detection of a weak contour by the RG model due to the high sensitivity of the segmentation to the initial contour and the similarity index. Afterwards, Nija et al. [36] put forward an approach based on the Statistical Region Merging (SRM) for detecting the OD border in retinal fundus images. Subsequently, they threshold the brightness value V of the converted SRM image to an HSV color space. Finally, a morphological operation combined with geometric analysis of the OD region was applied to segment the OD. Note that, the advantages of the thresholding techniques are the simplicity, the inexpensive computation and the interaction in real-time. Although, the use of the threshold value is critical and noise sensitive. Moreover, this type of methods ignores the spatial information in the retinal fundus image [37].

Regarding the region-based methods, they are proposed to segment the optic disc region. It divides the fundus image into several region based on the object, the intensity, or the color. The most used methods in the literature were the region merging, growing and splitting. The region growing method is the well-developed one in the fundus image segmentation. For example, Morales et al., [7] proposed an automatic segmentation of the OD focusing on mathematical morphology-based operations. In the preprocessing step, Principal Component Analysis (PCA) was used for combining the most important information of the RGB images in one grayscale image and then the different structures of the retinal image were separated. The OD segmentation was realized using a stochastic Watershed transformation, followed by a fitting step to eliminate non-OD regions (such as the blood vessels) by creating a

circular approximation of the OD contour. The Watershed transformation is based on the region growing technique. In addition, Guo et al. [12] used the HSL color space in the preprocessing and applied on it a morphological operation to remove the blood vessels. They also used the fractional-order Darwinian particle swarm optimization technique to segment the image by extracting the brightest region. Finally, the detected borders of the OD were smoothed by considering the size of the major/minor axis of the surrounding region. Moreover, Yi et al. [40] improved an OD segmentation algorithm based on a modified particle swarm optimization. In order to optimize the contour of the segmented optic disc, an iterative update of the position of the particles is applied.

Besides, an improved image processing algorithm was proposed by Ramani et al. [34]. The authors introduced a sequence of preprocessing methods represented in image resizing, binary mask generating, morphological erosion, element wise multiplication and Gaussian filtering. Afterwards, the authors used the region-based pixel density calculation to locate the OD. In order to segment the OD, they proposed an improved CHT followed by super-pixel red-channel segmentation. In the approach presented by Kim et al. [41], a morphological operation was applied in order to remove the blood vessels in a pre-processed image by noise removal and contrast enhancement. Next, the OD was extracted using image features such as the shape, intensity, and size. The region-based methods are more recommended to extract the real boundary of the optic disc since they start from the center point to the outer region. Moreover, they give a high result in the optic disc segmentation task. However, it is hard to formulate the stop condition of the algorithm. In addition, a precise segmentation depends on the choice of the initial seed [37].

Concerning the template-based methods, they consist of comparing a model with a set of candidates and determining the best-matching. Indeed, For the OD detection, Chalakkal et al. [15] used the histogram-based template matching and maxima sum of vessel information. The CHT was used in this approach to segment the OD. In addition, the macula was determined by heuristic parameters applied in a series of image processing phases and the fovea was detected using a morphological operation. Moreover, to detect the OD in color fundus images, Kaya et al. [42] use a cuckoo search algorithm with a structural similarity index measure. In this work, the average OD values of a dataset were computed followed by a search algorithm. Another example of the usage of template-based method is presented in Ref. [43]. A novel approach based on the bat meta-heuristic algorithm was proposed by Abdullah et al. [43] to detect the OD. Shalchi et al. [44] proposed an OD detection method based on the Grasshoppers technique by evaluating the fitness function, checking and updating the optimal position of individual Grasshoppers. In this technique, the authors removed the vessels using morphological operations in grayscale images, and then applied the bat algorithm to optimize the threshold value of the image for the OD localization. Finally, the ellipse fitting was applied to smooth the results. To locate the optic disc in retinal fundus images Kumar et al. [45] proposed a novel Jaya algorithm based on a novel fitness function. The template-based method is the most compendious optic disc segmentation method. Regardless, it is sensitive to noise [18].

Regarding the clustering techniques, they can describe each segment in the image by its shape and texture in order to classify the pixels. The commonly utilized methods are the fuzzy clustering methods, the k-means clustering methods and the expectation maximization method [46]. These techniques are suitable for real problem. Nevertheless, it is hard to determine the membership function [37].

Concerning the pattern recognition techniques, they are composed by two steps: the development of the decision rules and the classification of fundus image using these rules. Abdullah et al. [47] proposed the use of the mathematical morphology to remove the vessels and in order to enhance the OD region. They approximated the OD center by the CHT. Finally, the OD boundary is determined with the grow-cut algorithm by starting with the detected OD center point in the region to grow. The

authors proposed an effective technique with a complete detection and segmentation process required for automatic systems. However, this method was not sufficiently efficient with some databases. In addition, the method suggested by Naqvi et al. [17] used the OD homogenization to segment the OD when it is smooth or discontinuous because of the presence of a disease. For that, the authors build OD boundary by local Laplacian filtering followed by major vascular structure inpainting. Eventually, the OD border is detected using the gradient-independent active contour estimation. The advantage of pattern recognition techniques is the creation of a relationship between the input and the output. However, these methods are restricted on shape feature and more complicated compared to the previously cited methods [37].

Recently, Deep Learning (DL) techniques have been utilized with medical images after the fast evaluation of the Convolutional Neural Network (CNN). The DL architecture has been applied to detect and segment the OD. This architecture aims to keep away from false positive detection. Bright regions, such as exudates and blood vessels, are the two main causes of the false positive detection.

The work of Fan et al. [16] presented a supervised OD contour extractor, which was trained using structured learning. After the training stage by a Random Forest (RF) classifier, the authors applied a threshold to obtain a binarized image of the OD. A CHT was accomplished for estimating the circular shape of the OD boundary. This work has been one of the most competitive approaches with high performance. However, the analytical choice of the threshold and the lack of variety of fundus images for training led to a limited generalization of blurring images.

AlBander et al. [48] proposed an OD and OC segmentation method based on DL, besides the FC-Dense network whose classification was adapted to a fully convolutional network in order to diagnose glaucoma in retinal fundus images.

For the detection of the OD border, Rehman et al. [18] proposed a feature-based approach in each super-pixel of the fundus image. The selection of used features was realized by analyzing and comparing four benchmark classifiers.

Diaz-Pinto et al. [49] employed five different CNN models to classify fundus images into and glaucomatous. High performance was achieved with the Xception network model by training using images from different public databases.

A CNN architecture was employed by Joshi et al. [50] to segment the OD region. In the work of Latif et al. [51] a Shallow CNN is utilized to detect the optic disc.

A multi-adversary network (multi-ADV) and a single Fully CNN with skip connection were proposed by Saha et al., [52] to predict the classes in retinal fundus images. In this work, the authors used a separate weakly labeled dataset in the training phase to segment retinal anatomy and pathology such as the OD, microaneurysms, hemorrhages, and exudates. However, only 121 images were used in this approach.

In the literature we also find the approach of Yu et al. [53] based on a combination of the deep CNN and the generative adversarial networks in order to segment the OD and the OC. In addition, Carvalho et al. [53] used a hybrid machine learning model to segment the optic disc and the optic cup in retinal fundus images. For that, a conditional generative adversarial network was utilized to ensure fast and precise results.

Hervella et al. [55] proposed a multi-task architecture to simultaneously achieve the OD segmentation and the glaucoma classification. In the training process, they combined the image-level and pixel level labels. A weak label-based Bayesian UNet was proposed by Xiong et al. [56] to segment the optic disc. Since the pixel-level optic disc annotation needs a large time, the authors utilized an annotation based on Hough transform.

Wang et al. [57] used a U-Net model based coarse-to-fine deep learning framework to segment the OD. This approach integrated image contrast and the retinal vessels to achieve the objective. In the work of Gu et al. [58], a context encoder network (CE-Net) was presented to extract high-level features for medical image segmentation. To provide

better segmentation results, a combination of features and spatial information in the decoder of the conventional U-network was used by Tabassum et al. [59]. Lu et al. [60] proposed a technique to generate the pseudo-ground-truth using the Grab-Cut method which was utilized for training a modified U-network model. After all, the authors used little ground-truths to fine-tune the presented model. In Ref. [19], after detecting and removing the blood vessels a decision tree classifier was trained based on the free-vessel images and the OD annotations. Specifically, the training phase aimed on identifying an adaptive threshold value to segment the OD. High performance was observed with retinal color fundus images having exudate or illumination. In the approach of Hasan et al. [61], an encoder-decoder network (DRNet) model was suggested to locate and segment the OD centers and the fovea. the authors presented a residual skip connection to compensate the spatial information. Besides, Shi et al. [62] proposed a recurrent skip network formed by a skip connection and a set of three convolutional blocks. Khaing et al. [63] segmented the OD to detect the glaucoma in retinal images taken by mobile phone. They used the alternated deflation-inflation gradient vector flow model and the exclusion method to improve the precision of extracting ODs. The work of Escorcia et al. [64] was based on the Modern Portfolio Theory of Markowitz combined with a mathematical optimization model to create an original color fusion model of six channels by calculating the optimal weight for each color channel in the training phase. Subsequently, they fused the weighted color channel and applied it in the testing phase. Two segmentation approaches were used, which were Extended Minima Transform (EMT) with a Hough Transform (HT) and a Graph Cut (GC). Specifically, the GC method proved the high performance with the minimum computational time. Zhao et al. [65] combined the attention U-network with transfer learning.

In Zhang et al. [66] the authors proposed the use of a transformable attention U-network model with the aim of segmenting the OD and the OC in fundus images. An attention model including with two discriminators is proposed in order to extract fixed features in different datasets.

In the work of Zhou et al. [67] a semi supervised extreme learning machine combined with a low-rank representation is introduced to detect the optic disc.

In the paper of Wang et al. [68] the region of the optic disc is detected directly, without the localization stage. For that, the authors constructed the feature matrix by extracting edge, color and texture feature from each super-pixel in the image. Then, they created a hierarchical segmentation tree utilizing the correspondence between features of super-pixel and the spatial connectivity. Finally, they were decomposed the matrix of features was decomposed to become a sparse matrix using the combination of the structured matrix decomposition model and the fully convolution neural network.

A region proposal network was used by Huang et al. [69] in order to produce multiple regions proposal of the optic disc, and the region of interest with the highest probability was selected as the OD region. This method was detected the bounding box of the optic disc without the need of *a priori* knowledge on the optic disc property.

The segmentation of the optic disc is an essential step to detect the glaucoma. In fact, a great number of articles in the literature presented novel methods for OD segmentation in order to detect the glaucoma. Some of this research work used the machine learning algorithm to detect the glaucoma. More specially, the identification of the symptoms of glaucoma in retinal fundus image through the machine learning techniques need to extract features from image with high quality [70]. A versatile Deep Learning models was presented in Ref. [71] and implemented on several databases in order to detect the glaucoma in retinal fundus images. In addition, the authors of [72] propose a method that remove the blood vessels through the multistep closing morphological operation, and locate the optic disc region by applying the maximally stable external region.

Each algorithm described above has a limitation that will be discussed below. For instance, the algorithms based upon the OD

appearance, like the size and the shape are prone to detect false regions such as the exudates or the blood vessels instead of detecting the OD since it is difficult to specify the threshold value and employ a reliable edge detection method. Similar problems appear in approaches using these methods in the preprocessing step. Furthermore, the large training time of algorithms based on learning is one of the drawbacks of these approaches besides the use of high-end computing resources, which is impractical in several clinical applications. These two drawbacks limit the use of these algorithms in real-time diagnosis. In our paper, the proposed method aims to tackle this weakness.

3. Proposed method

The OD segmentation becomes a problematic since the disc borders are not always clearly defined. Therefore, we propose an OD segmentation method that includes two phases.

The first phase aim to locate the OD through four steps. First, a haze reduction was used as a preprocessing step to improve the quality of the fundus image. Second, a blood vessel extraction was proposed in order to eliminate this hinder front of the OD segmentation. Third, a saliency mask was applied in the vessel inpainted image to emerge the regions of interest. Forth, a geometric analysis is chosen to select the object of the localized OD.

On the other hand, the second phase is to determine the exact boundary of the optic disc. For that, a preprocessing step of the localized image was used especially for decreasing the brightness of the detected region so that we can extract other salient regions. Then multiple saliency masks were applied to specify the salient areas adjacent to the region of the detected optic disc. These areas may belong to the optical disc. For this reason, the OD boundary candidates were selected. Finally, an ellipse fitting step is necessary to delineate the border of the optic disc. Fig. 1 presents the flowchart of the proposed approach for OD localization and segmentation.

3.1. OD localization

The first step of the proposed method consists of the preprocessing step which is based on the haze removal algorithm. Then, a set of methods are employed on the preprocessed images for OD localization. In fact, the optic disc identification is composed by eliminating the artifact noise, inpainting the extracted blood vessels, applying a series of morphological operations, and finally analyzing the geometry.

Algorithm 1. summarizes the entire steps used for extracting the blood vessels and locating the optic disc.

Algorithm 1	
Input:	$I(x, y)$ RGB fundus image
Output:	Localized optic disc
Preprocessing	1: Apply the haze removal algorithm ($H(x, y)$) using Eq. 1
Blood vessels extraction	2: Select the green channel ($H_G(x, y)$)
	3: Apply the contrast limited adaptive histogram equalization algorithm ($C(x, y)$)
	4: Apply the Gaussian filter ($G(x, y)$) using Eq. 3
	5: Apply a linear structuring element with a length of 150 pixels and eight orientations from 0° to 360° in steps of 45° using Eq. 5($M_1(x, y), \dots, M_8(x, y)$)
	6: Sum up the eight responses using Eq. 4 ($M_{total}(x, y)$)
	7: Apply the Bernsen thresholding to extract the blood vessels ($V(x, y)$)
	8: Apply the Laplacian filtering on the red channel of the preprocessed image using Eq. 9 ($L(x, y)$)
	9: In-paint the extracted blood vessels using Eq. 7, Eq. 8 and Eq. 10
Optic disc localization	10: Apply the supremum of opening using Eq. 11 ($S(x, y)$)
	11: Apply the morphological reconstruction using Eq. 12 ($M(x, y)$)
	12: Apply the regional maxima ($R(x, y)$)
	13: Select the region of interest to locate the OD by a geometric analysis ($Loc(x, y)$)

3.1.1. Haze reduction

The fundus imagery presents an important noise artifact called the haze [73] which is defined by a region with varied contrast and less visibility. This image property of the fundus image photography produces difficulties in the OD localization task. In order to enhance the OD region of noisy images, a haze removal method is used to restore the original color of the retinal structures. The used dehazing algorithm recovers the scene radiance using the dark channel prior method [74] and estimates the atmospheric light and the transmission map. Fig. 2 shows the impact of the dehazing algorithm on the appearance of the OD and the vascular structure in color fundus images. The haze removal function H is expressed as shown in Eq. (1):

$$H(x, y) = \left[(I(x, y) - A) / (\max(T(x, y), t_0)) \right] + A \quad (1)$$

where: I is an input colored image, A is an estimated atmospheric light by the dark channel prior, T is an estimated transmission, x and y are the coordinates points of an image and t_0 is typically fixed to 0.1.

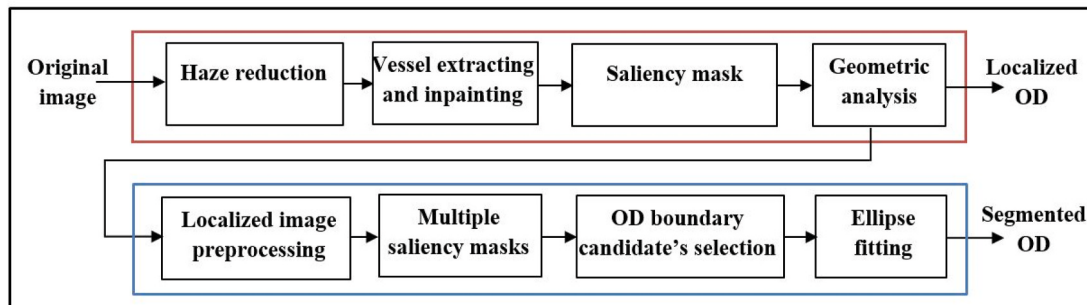


Fig. 1. Block diagram of the proposed approach for OD localization and segmentation.



Fig. 2. Impact of dehazing method, (a) original image, (b) after dehazing algorithm.

As mentioned in Fig. 2 after applying the dehazing algorithm on a color fundus retinal image, the OD becomes brighter, besides the blood vessel's structure, the bright lesions, and the OD borders will be clearer.

3.1.2. Vessel extracting and inpainting

Removing the blood vessels increases the efficiency of OD detection process. Actually, these vessels must be, first, localized in order to remove them. Fig. 3 shows the proposed process of blood vessel detection and elimination for fundus preprocessed image.

Vessel extraction is based on the application of the histogram processing technique CLAHE on the green channel of the RGB color space, followed by Gaussian filtering, adapted morphological operations and finally Bernsen thresholding. On the other hand, inpainted vessels are obtained by injecting into an inpainting process the output of the Laplacian filter applied on the red channel, and the output of the extracted vessels using the Bernsen thresholding.

3.1.2.1. Color channel selection. The color image present three type of color channels; Red, Green and Blue. We can notice that the haze-free colored image $H(x,y)$ is composed by three channels and it is described by $H(x,y) = [H_R(x,y), H_G(x,y), H_B(x,y)]$; where x and y are the points' coordinates of an image and $H_R(x,y)$, $H_G(x,y)$ and $H_B(x,y)$ represent the red, green and blue channel of the image, respectively.

Regarding the state of the art, several studies have shown that most of vessels are significantly evident and more prominent within the green channel of the haze-free images ($H_G(x,y)$) [3,19,34,35]. Moreover, the red channel is characterized by high contrast regions which lead to the hard differentiation between the OD and the bright lesions such as exudates. On the other hand, the blue channel presents regions with low contrast which means that it will hide nearly all the blood vessels. Therefore, to extract the vessels, a set of morphological operations can be applied on green channel of the free-haze image.

3.1.2.2. CLAHE. The retinal fundus image quality depends depending on the used device. Indeed, some images may be captured with low contrast, leading to the inability to extract some lesions. Therefore, the

use of the Contrast Limited Adaptive Histogram Equalization (CLAHE) method [75] is used in our work to obtain blood vessels with the highest contrast and OD regions brighter than other features. Instead of enhancing an entire image, CLAHE is a histogram processing technique that performs and enhances the contrast on each tile individually in the image. The tile is a small rectangular contextual region dividing the processed image. The algorithm of CLAHE consists first of dividing the images into three independent images R, G and B and, then, dividing each image into tiles. Second, after calculating the contrast limited histogram of each tile, the pixels over this value must be clipped and then redistributed the remain pixels. Third each region must be enhanced with a type of distribution (uniform, exponential or Rayleigh) in order to specify the desired shape of the histogram. Finally, all the images should be combined through a bilinear interpolation.

In our approach, 8×8 tiles are considered and the value of 0.01 as a contrast improvement limit along, thus, to avoid background noises. Finally, the histogram of the output region must approximately match a flat histogram (uniform) Eq. (2).

$$Dist(x,y) = [Dist_{max} - Dist_{min}] \times P - Dist_{min} \quad (2)$$

where, $Dist_{min}$ is the minimum pixel value, $Dist_{max}$ is the maximum pixel value and P is the cumulative probability distribution.

By increasing the number of tiles and the enhancement limit value, the contrast of the background pixels will increase. Moreover, setting low values to these parameters affect a non-enhanced contrast of the OD region. From our analysis, to enhance the OD in the 11 databases we can say the chosen parameters' values are the most convenient.

3.1.2.3. Gaussian filtering. A 2D Gaussian filter is used in order to smooth the image by removing noises, to estimate the local background and to blur the small distraction such as small lesions and cotton wool spots and to estimate the local background. The 2D Gaussian distribution function is specified by a standard deviation value, noted sigma σ . The 2D Gaussian function is given by Eq. (3).

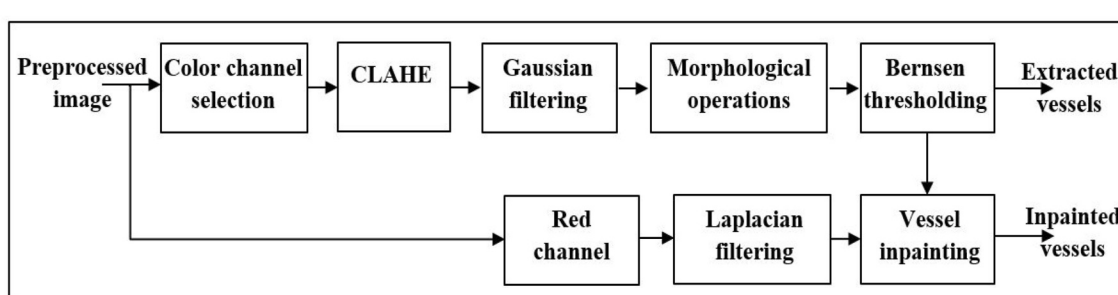


Fig. 3. Flowchart of vessel extraction and inpainting phase.

$$G(x, y) = \frac{1}{2\pi\sigma^2} e^{-\frac{(x^2+y^2)}{2\sigma^2}} \quad (3)$$

where, x, y are the point coordinates of an image-enhanced contrast and σ is the standard deviation of *Gaussian* distribution.

3.1.2.4. Morphological operations. The use of a high-pass filter produces some noise around the OD, which can be removed easily with the help of morphological operations. For that, a linear structuring element that has eight various orientations in steps of 45° from 0° to 360° is applied. A subtraction of the Gaussian filtered image from the response image of dilation and erosion in each orientation is performed. Finally, all the responses are summed up ($M_{total}(x, y)$) to turn out the retinal image's blood vessels [19].

$$M_{total}(x, y) = M_1(x, y) + M_2(x, y) + M_3(x, y) + \dots + M_8(x, y) \quad (4)$$

where, x and y represent the point coordinates of an image,

$M_i(x, y)$, $i = 1, 2, \dots, 8$ denotes the subtraction of the gaussian response, and the erosion of the dilated Gaussian filtered image is represented as follows:

$$\left\{ \begin{array}{l} M_1(x, y) = [(G(x, y) \oplus line(150, 0)) \ominus line(150, 0)] - G(x, y) \\ M_2(x, y) = [(G(x, y) \oplus line(150, 45)) \ominus line(150, 0)] - G(x, y) \\ M_3(x, y) = [(G(x, y) \oplus line(150, 90)) \ominus line(150, 0)] - G(x, y) \\ \dots \dots \dots \dots \dots \dots \\ M_8(x, y) = [(G(x, y) \oplus line(150, 315)) \ominus line(150, 0)] - G(x, y) \end{array} \right\} \quad (5)$$

where " $G(x, y)$ " is the Gaussian filtered image,

" \oplus " and " \ominus " are the dilation and erosion morphology functions, respectively, line (150, d), with $d = 0, 45, 90, \dots, 315$ is a linear structuring element with a length of 150 pixels and 'd' is the degree of the orientation of the line.

After a variation in the standard deviation constant of the Gaussian filter applied on a set of 100 images, $\sigma = 4$ gives us the most suitable extraction of blood vessels for all databases' images. Below this value, the obtained image is smooth; and above it, some image information is lost, as shown in Fig. 4. The response sums up images of morphological operation using a Gaussian filter having a standard deviation equal to 4 is depicted in (Fig. 5(b)).

3.1.2.5. Bernsen thresholding. The enhanced vessels image is binarized through a chosen threshold value. From our experiments and after testing other binarized algorithms such as the Otsu thresholding method, we can observe that the local gray range technique used by the Bernsen's thresholding technique [76] fits the best for extracting the region of interest used to localize the ODs for all the databases. This method uses the contrast threshold and the mean of the minimal and maximal gray values for each specific local window (as shown in Eq. (6)). The response of the Bernsen thresholding method is denoted by $V(x, y)$ in Eq. (7). The local window is centered in the point (x, y) and has a size of $(2w + 1)^2$. The used threshold $Th(x, y)$ is represented by Eq.

(6).

$$Th(x, y) = \frac{\min_{-w \leq k, l \leq w} M_{total}(x + l, y + k) + \max_{-w \leq k, l \leq w} M_{total}(x + l, y + k)}{2} \quad (6)$$

$$V(x, y) = \begin{cases} 0, & \text{if } M_{total}(x, y) < Th(x, y) \\ 255, & \text{else} \end{cases} \quad (7)$$

where $M_{total}(x, y)$, mentioned in Eq. (4), is the result of applying a set of morphological operations with x and y the points' coordinates of an image, and k and l are the x-axis and y-axis direction size of the window, respectively.

All the images in the databases were tested by varying the window size from 15 to 45. The selected sizes are 25 and 25 for the x and y axis directions, respectively.

3.1.2.6. Vessel inpainting. Vessels filling or inpainting is an important task to estimate the missing pixels of the vessels' regions. A simple and fast Laplacian transform is used ($L(x, y)$), which is a method based on the neighbor indexing technique. Using the eight neighbors of a missing pixel in the preprocessed image's red channel, the inpainting region with Laplace process can be interpreted as the average of adjacent pixel values. A red channel can be used in this process since it gives a better view of the OD. The equation of the Laplacian transformation of the red channel of the haze-free image ($H_R(x, y)$) using eight neighbors is expressed in Eq. (10). This Laplacian transformation and the binary image of extracted vessels ($V(x, y)$) are used to obtain the vessel inpainted image ($VI1(x, y)$) as expressed in Eq. (8). Nevertheless, a bright lesion or an artifact near to the OD can be treated as an OD. For that, another vessel filling task based on the preprocessed image's green channel ($H_G(x, y)$) and the binary image of extracted vessels is used to eliminate these bright regions. The output image of inpainted vessel is expressed by $VI2(x, y)$ in Eq. (9).

$$VI1(x, y) = inpaint(L(x, y), V(x, y)) \quad (8)$$

$$VI2(x, y) = inpaint(H_G(x, y), V(x, y)) \quad (9)$$

with: $L(x, y)$ is the Laplacian of $H_R(x, y)$, which defined by Eq. (10):

$$L(x, y) = \frac{[H_R(x - 1, y - 1) + H_R(x - 1, y) + H_R(x - 1, y + 1) + H_R(x, y - 1) + H_R(x, y + 1) + H_R(x + 1, y - 1) + H_R(x + 1, y) + H_R(x + 1, y + 1)]}{8} \quad (10)$$

where ($H_R(x, y)$) is the red channel of the haze-free image and x and y are the points' coordinates of an image. The Laplacian of each pixel consists of summing the intensity of the desired neighbors' pixels and dividing the sum by the number of the neighbors. In our case, it is the 8 surrounding pixels. A combination of these two images with an appropriate weighting [77] is proposed and presented by Eq. (11). Fine adjustment of the value of the parameter α will be discussed in section 5.1 in order to have clear OD without considering the bright lesions, as illustrated in

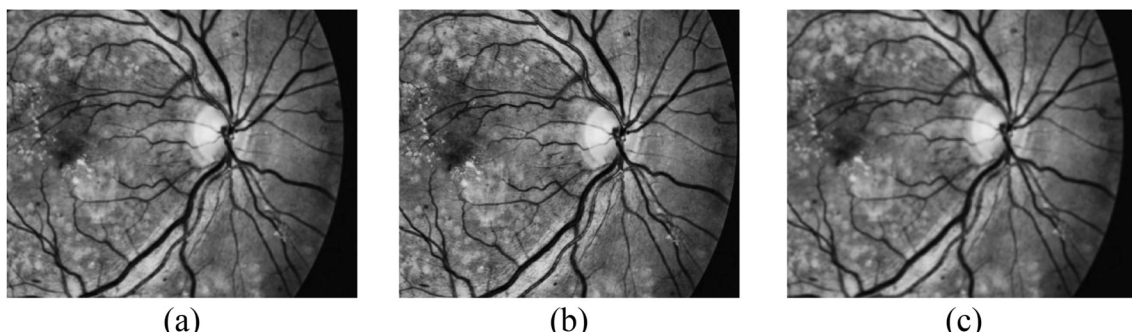


Fig. 4. Variation of standard deviation of Gaussian filter: (a) $\sigma = 4$, (b) $\sigma = 2$ and (c) $\sigma = 6$.

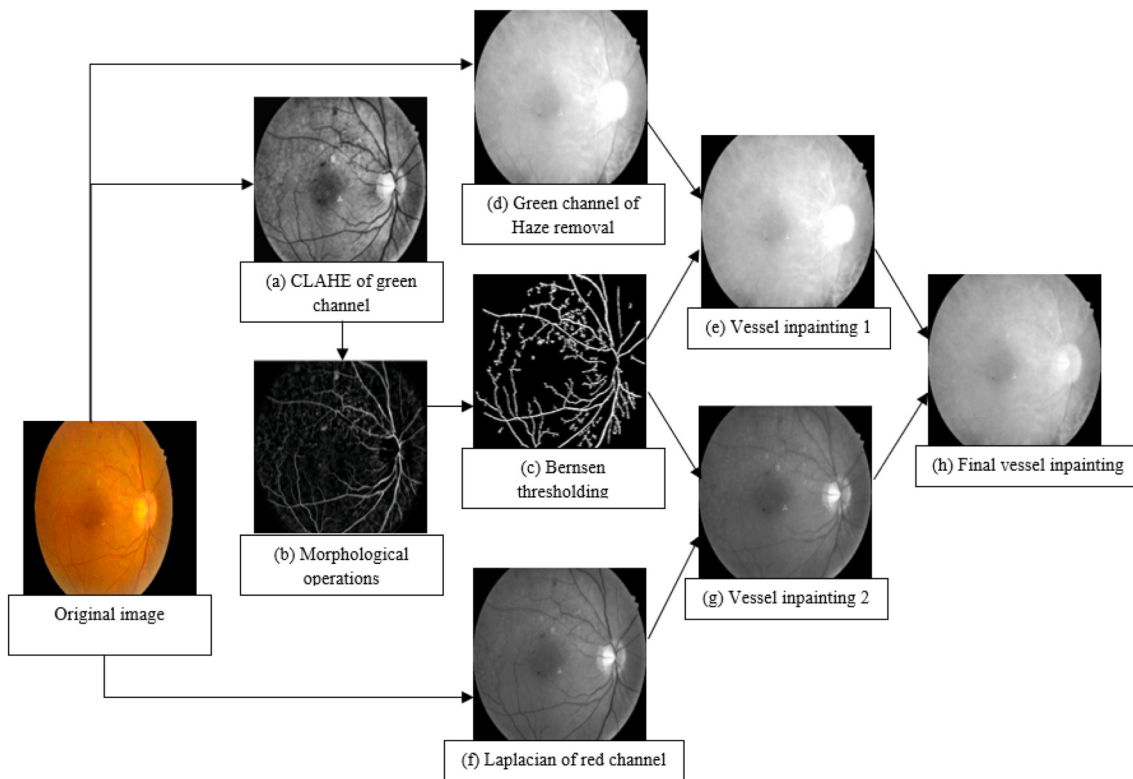


Fig. 5. Process of extracting and inpainting vessels.

Fig. 5.

$$VI(x, y) = \alpha \times VI1(x, y) + (1 - \alpha) \times VI2(x, y) \quad (11)$$

The main idea in assigning the major weightage to the vessel inpainted image based on the red component is the conservation of any variation in the red channel and that is across the OD boundary, as well as negligence of the variation across the blood vessels that is present powerfully in the vessel in-painted image based on the green channel. Fig. 5 shows an example of the result of vessel inpainting images.

Fig. 5 illustrates a critical case where the optic disc is surrounded by a bright lesion (as presented in the original image). In this case it is very important to segment the optic disc with high precision to ensure that the application of any treatment does not approach to the optic disc, which can cause the blindness. After the application of the vessel inpainting method based on the green channel of free-haze image, the OD region and the bright lesion which is close to the OD become brighter. While the second method of vessel inpainting based on the Laplacian of the red channel accentuate the OD and the OC. Whereas, the combination of these two methods of vessel inpainting eliminate the bright lesion.

3.1.3. Saliency mask

A saliency mask is presented in this paper to extract the salient region in the retinal image represented by the bright regions. Our saliency map

consists of three steps. First, the supremum of opening is applied on the vessel-inpainted image. Second, a morphological reconstruction is used to emerge the compactness of bright region without missing the local intensity maxima. Finally, a regional maxima method is applied to isolate the salient region of interest by generating a black and white image. After extracting the retinal image's structural vessel, the OD center is automatically extracted in this stage by the phases explained in this section. Fig. 6 describes the process of the proposed saliency mask.

3.1.3.1. Supremum of opening. The first step to create the saliency mask aim to enhance the contrast in the image. In order to determine the OD center in a vessel-inpainted image, we attempt to extract the regions of interest based on local region maxima. Since the morphological opening is able to “break” thin isthmuses, eliminate narrow protrusions and smooth the contour of an object [78] where a supremum of opening is used in our process. It is defined by the following expression Eq. (12).

$$S(x, y) = \bigcup_{d=0}^{37} [(VI(x, y) \ominus se) \oplus se] \quad (12)$$

where $se = line(l, d \times 10)$

A set of 38 linear structuring elements with a specific length (l) and various line orientation angle ($d \times 10^\circ$) from 0° to 350° . The length of the structuring elements is required to be large enough to remove large vessels, small lesions, hemorrhages, cotton wool spots and

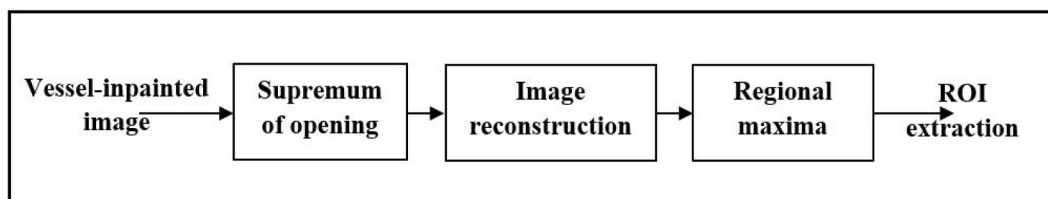


Fig. 6. Process of saliency mask.

exudates.

The line orientation angle is fixed after some tests. In fact, all the images were tested using a disk structuring element and a line structuring element to choose between them. Considering the disk structuring element, various radius varied from 2 to 50 were applied. Considering the line structuring element, we have tested various length values and angle values; where the length varied from 5 to 100 and the angle is from 5° to 90°.

Based on our experimental results, the pathological distraction such as hemorrhage, exudate and cotton wool spots are smoothed by the line structuring element, unlike the disk structuring element which give us worse results. These pathological distractions having a circular shape may mislead the optic disc segmentation. We can conclude that from our conducted experiments, that the line orientation angle is varied in steps of 10°, whereas the line length depends on the retinal image's resolution. It is unrealizable to apply a morphological opening using a line with a length of 100 pixels for an image of 600 × 400 pixels like in the HRF database. These parameters will reduce the number of regions of interest, which leads to increase the processing time.

3.1.3.2. Morphological reconstruction. The obtained supremum of these different openings will be used as a mask to reconstruct the retinal image. A fast hybrid grayscale Morphological Reconstruction (MR) [79] is performed to isolate and localize the salient region of interest. A simple thresholding would miss some local intensity maxima characterized by a varied absolute intensity, which will be determined by a MR. The MR is formed by a repeated dilation of a marker image, which is a result of the supremum of opening, until it fills the mask Eq. (13), which is represented by the vessel inpainted image (Fig. 7(c)). The MR can enhance the compactness of bright regions such as the OD, the bright lesions and the contrast variation throughout the blood vessels. The obtained image is a grayscale image which will be binarized by localizing the regional maxima.

$$M(x, y) = \text{reconstruct}(S(x, y), VI(x, y)) \quad (13)$$

3.1.3.3. Regional maxima. By analyzing the retinal image, it can be clearly observed that every OD region has one Regional Maxima (RM). The RM extraction [80] can convert grayscale reconstructed images into binary images without using any specific predefined threshold. The resulting RM is a connected component with a constant intensity value, such that every pixel in the external boundary has a strictly lower intensity value. It is the process of extracting the regions with high contrast in the retinal image, which differ from the local maxima. Specifically, all the pixels in the RM are local maxima; however, the reverse is false. Fig. 7 depicts an illustrative example of the results of RM of one retinal image in the used databases.

3.1.4. Geometric analysis

The regions of interest are acquired to decrease the processing time and reduce the area of the processing zone instead of analyzing the whole image. Each connected region has its own label to differentiate between objects. After binarization and regional maximal extraction, in a selected area, the centroid of the object having a maximal circularity value and a specific major axis length range is considered as the OD centroid. The computed circularity can be calculated using Eq. (14).

$$C = (4\pi \times Ar) / (P^2) \quad (14)$$

where: Ar is the area of the region and P is its perimeter.

Some authors such as Khan et al. [35] chose to localize the OD using the calculation of the minimum of eccentricity, which will not be suitable with the considered databases of fundus images containing glossy areas like the exudate. Fig. 8 shows an example where the circularity calculation is better than an eccentric method. In Fig. 8 (b), after eliminating the objects labeled 2, 6 and 7 by the criterion of major axis length range, the minimum of eccentricity is given to the object labeled 3, while the object labeled 1 which has the maxima of circularity is the desired OD region.

The defined zone refers to a rectangle located in the center of the retinal images whose sides are the length of the image and the three fifths of the width of the original image. It is worthwhile to stress that all

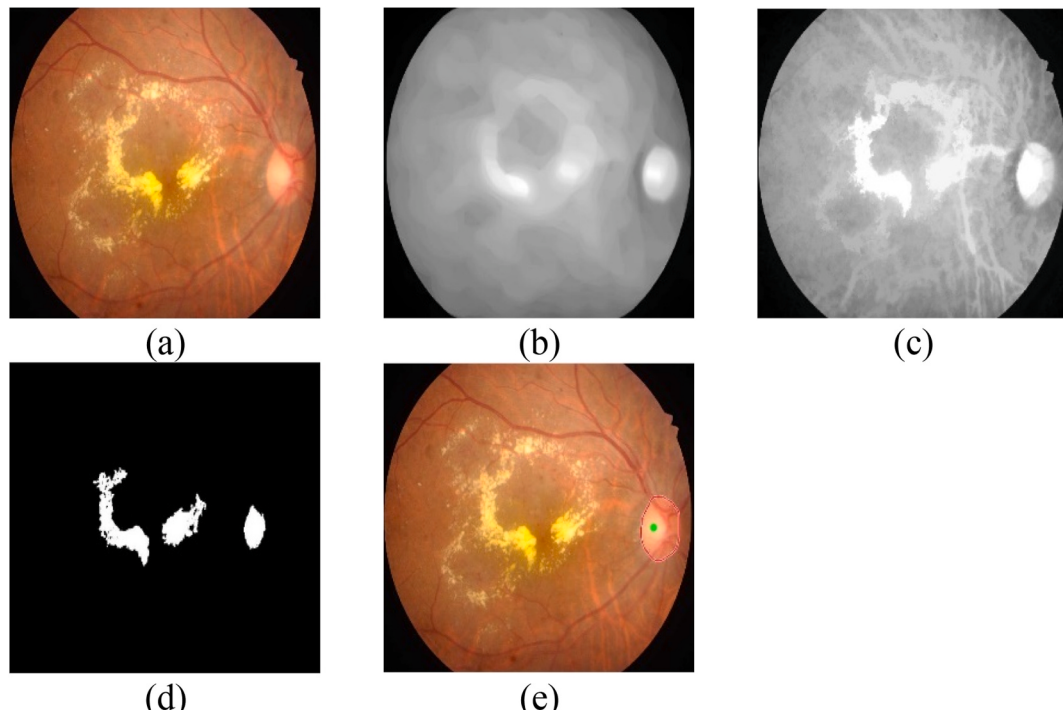


Fig. 7. Saliency mask, (a) original image, (b) supremum of opening, (c) morphological reconstruction, (d) regional maxima, (e) geometric analysis and optic disc localization with green dot representing detected optic disc centroid.

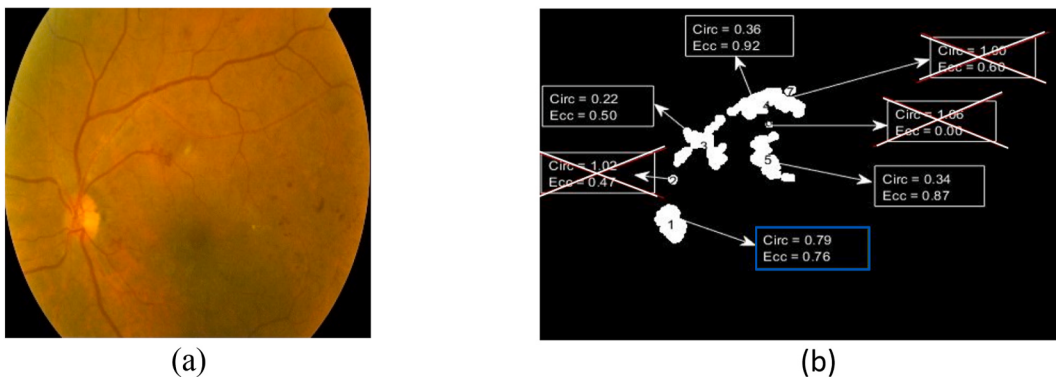


Fig. 8. Geometric analysis: Example for choosing circularity parameter instead of eccentricity, (a): original image, (b) geometric analysis.

the centroid of the optic discs of our databases are inside this area. The defined region can minimize the number of false positive pixels. It can also decrease the processing time. The range of the major axis length is proposed to be $M_f/2 = R_{est} \pm \beta \times R_{est}$ after various tests, where R_{est} is the estimated radius of the OD in each database, and from our experiments, $\beta = 0.66$ is apt for the whole database as a result of diverse measures from 0.1 to 1.9, to eliminate both big and small objects compared to the estimated OD radius. In this work, the mathematical model proposed in Ref. [81] is applied for estimating the OD radius in retinal fundus images using the procedure and the equation *Eq. (15)* given in Ref. [81]:

$$R_{est} = \sqrt{\left(D_{OD}/2\right)^2 / \left(A_{fov}/N_{fov}\right)} \quad (15)$$

where D_{OD} is the average diameter of a human optic nerve, A_{fov} is a retinal area of the FOV and N_{fov} is the number of pixels in the FOV. More specifically, after analyzing a set of cases, the authors in Ref. [82] concluded that the vertical and horizontal disc diameters were respectively in the range of [1.69; 2.07] and [1.57; 1.95]. Accordingly, by choosing the mean of two intervals, D_{OD} is fixed at 1.88 mm. According to Ref. [83], the value of the retinal area A_{fov} depends on the value of the FOV angle, as mentioned in Table 1 [83,84]. In fact, the retinal area (A_{fov}) is calculated using the following equation:

$$A_{fov} = 2\pi \times r^2 \times \left(1 - \cos \frac{\theta_e}{2}\right) \quad (16)$$

where:

$$\frac{\theta_e}{2} = \frac{\theta_v}{2} + \sin^{-1} \left(0.51 \times \sin \frac{\theta_v}{2}\right) \quad (17)$$

with $r = 11\text{mm}$ and θ_v is the visual angle.

To compute the number of pixels (N_{fov}) within some FOVs, the FOV diameter is determined by analyzing the intensity of the image diagonal in the red channel [85].

3.2. OD segmentation

The OD boundary extraction phase is performed on the localized region. All the correctly localized fundus images can be put down with a preprocessing step, an improved saliency-mask extraction having a specific bounding circle around the OD localized centroid, an OD boundary candidate's selection, and an Ellipse fitting algorithm. The

details of segmentation are presented in this section. Algorithm 2 summarizes the entire steps used for segmenting the optic disc.

Algorithm 2.

Algorithm 2

Input: $Loc(x, y)$ binary image of the located optic disc
Output: Segmented optic disc

Optic disc segmentation

- 1: Fill the located optic disc region by his minimum intensity in the red channel of haze free image using *Eq. 15* ($F(x, y)$)
- 2: Fix three different lengths of linear structuring element to be used in the saliency mask
- 3: **for** each length **do**
- 4: Calculate the supremum of opening using *Eq. 12*
- 5: Calculate the morphological reconstruction using *Eq. 13*
- 6: Apply the regional maxima
- 7: **end for**
- 8: Create a bounding circle (BC) around the centroid of the located optic disc
- 9: Find the object that have the centroid inside the BC
- 10: **for** each object **do**
- 11: Find the objects that have a specific major axis length
- 12: **end for**
- 13: Fuse found objects
- 14: **if** there is only one object
- 15: Apply morphological opening with disk structuring element
- 16: **else**
- 17: Apply morphological closing with disk structuring element
- 18: **end if**
- 19: Extract the centroid, the orientation, the major and the minor axis length of the segmented region
- 20: Draw an ellipse surrounding the segmented region

Table 1
Relation between visual angle and retinal area.

Visual angle (°)	10	15	20	25	30	35	40	45	50	55
Retinal area (mm ²)	6.7	14.8	26.2	40.7	58.3	78.8	102.2	128.2	156.7	187.6

$$F(x, y) = [loc(x, y) \times Min_{Loc}(x, y)] + H_R(x, y) \quad (18)$$

where: $H_R(x, y)$ is the red channel of the initial haze free image, $loc(x, y)$ is the binary image of the located OD, $Min_{Loc}(x, y)$ is the minimum intensity of the convolution product of the binary image of the located OD and the red channel of the initial haze free image. It is defined by:

$$Min_{Loc}(x, y) = \min(loc(x, y) \times H_R(x, y)) \quad (19)$$

A localized OD preprocessing step is proved after experimental tests. The use of minimal, maximal, mean, and median intensities of the localized OD region in the blue, green, and red channels of preprocessed image are evaluated on all images of the 11 databases. The combination of the minimal intensity in the red channel of the preprocessed image is finalized from our experiments. This is explained by the fact that in the red channel the OD border are clearer, and the minimum intensity can improve the extracted regions of interest of the next step in order to show the other non-determined regions of the OD.

3.2.2. Numerous saliency masks

In this part of the algorithm, we aim to improve the extracted region after the OD localization method and to enlarge or reduce this region for the sake of faultiness segmentation. For that, a combination of various saliency masks is used. As previously explained in section 3.1.3, the saliency-mask generation consists in three steps: supremum of opening, morphological reconstruction and regional maxima. A set of three saliency masks is used and differentiated by changing the length of the line structuring element in the supremum of the opening step. By modifying this length, a group of regions is produced with different sizes, as shown in Fig. 9. To specify more, the line in the OD localization section is longer than the used line in the OD segmentation phase. In fact, if this structuring element is long, it selects a large area (represented by the located OD region), else, it allows us detecting the missing objects from the optic disc and segmenting all the objects. All the components of the optic disc are then detected. The orientation angle is varied from 10° to 90° in steps of 10° for the supremum of opening by applying 38 directional morphology openings on the preprocessed localized image.

In Fig. 9 multiple saliency masks are implemented to form all parts of the OD region. The black objects, which are the result of saliency mask with a small length of line in the supremum of opening step, represent the vessels cross regions in the OD. While the blue object, which is created by a larger length, characterizes the internal region of the OD.

3.2.3. OD boundary candidates' selection

The processing of the obtained regions of interest covering the whole image can increase the time processing and the inaccuracy of the proposed algorithm by choosing fault regions, hence, the need to use a bounding circle around the centroid of the localized OD. To make the OD shape circular with an estimated radius, the bounding circle containing

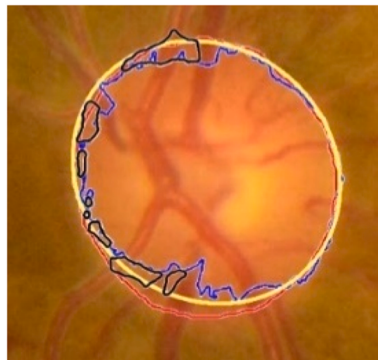


Fig. 9. Result of multiple saliency masks of several objects to form the OD; blue & black: objects in each saliency mask; yellow: the final segmented OD; red: the ground-truth.

the regions of interest should have a radius of $R_{est} + \epsilon$, where the centroid of objects having a half major axis length in the range $[R_{est}/4; 3 \times R_{est}/2]$ is extracted out; this range is chosen after heuristic tests. Two cases are produced: a single region of interest or several regions. In the first case, a morphological operation of opening by a disk with a radius of 15 pixels is necessary to smooth the border of the detected object. In the second case, several objects may belong to the OD. In addition, the existence of noises, small remaining vessels or dark inpainted vessels separate these objects. In this case, we try to concatenate these regions by a morphological closing operation with a disk of a radius empirically set as 15 pixels, which is approximately the width of a vessel, followed by an opening of a small disk to smooth the borders of the obtained object. It is worth noting that the selected object must have half of the major axis length nearest to the R_{est} , compared to other objects. Finally, it is necessary to remove the small regions outside the detected objects. Fig. 10 shows an example of each case and the segmented OD in different databases.

In Fig. 10(a) the blue and magenta (purplish red) objects represent the selected candidates, after a morphological closing these objects are fused to form the segmented OD. Although, in Fig. 10(b) the only selected blue object is appeared, a morphological opening is needed to smooth the OD region.

3.2.4. Ellipse fitting

After extracting the OD region (and even that the morphological operation cannot be done with a very big disk radius because this will drain a lot of information), the OD boundary has an irregular shape due to vessels removal. To estimate the correct OD region and mitigate the noise effects produced by the vessels outside as well inside OD region, the ellipse fitting is computed because the OD is found to take the form of an ellipse or a circle, which is a particular case of an ellipse. Therefore, the OD boundary is approximated as an ellipse. We have determined the ellipse that has the same second moments as the detected region. This ellipse is basically characterized by its centroid, its major and minor axes length, and its orientation. In fact, the lengths of the axis are given by the eigenvalues of the covariance matrix and the orientation is the angle between the horizontal axis and the major axis of the ellipse.

It is noticeable that in some cases when the OD is in the border of the FOV of the retinal image within the local database, this step can not be applied, and the detected object will be kept. Fig. 11 shows an example of the final segmented OD.

Note that, the ellipse fitting produces a binary image and in order to distinguish the segmented contour (in blue) and the ground-truth contour (in yellow) we have superposed the contours on the original image in Fig. 11. The OD is in the border of FOV in Fig. 11(a) and the elliptic shape of the OD is not shown, that's why the previously extracted object is maintained, whereas an ellipse fitting is necessary in Fig. 11(b) to get the usual elliptic shape of the OD.

4. Metrics and materials

4.1. Metrics

The OD localization proposed method for the 11 databases is implemented and the localization accuracy is calculated for each database. The accuracy rate of a particular database refers to the percentage of images where a proposed algorithm may correctly identify the OD as expressed in Eq. (20).

$$AccRate = C_{lod}/T_{im} \quad (20)$$

where C_{lod} represents the correctly localized OD, and T_{im} refers to the number of images inside the evaluated database. An OD is considered correctly localized when its centroid is inside the OD boundary of the ground-truth [84].

The performance of the proposed OD segmentation algorithm is



Fig. 10. Selection of OD boundary candidates: (a) grouped regions (b) single region; blue & magenta: selected candidates; green: OD segmentation; red: ground-truth.

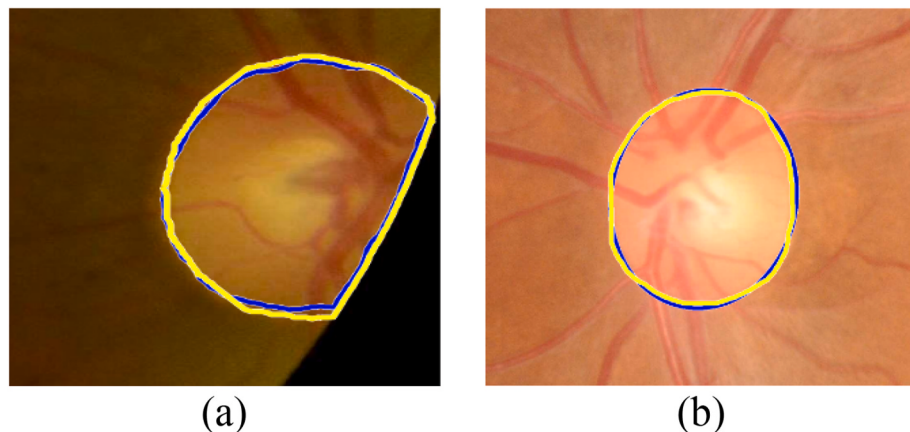


Fig. 11. OD segmentation: (a) without the use of the ellipse fitting in case of OD on the border of the field of view (b) with ellipse fitting. Blue: OD segmentation result overlaid on original image, yellow: Ground-truth overlaid on original image.

assessed as a function of seven standard performance metrics: Accuracy (Acc), Dice Coefficient (DC), Jaccard Coefficient (JC), F-score (Fs), Sensitivity (Se), Specificity (Sp) and Precision (Pr).

To calculate these metrics, the values of True Positive (TP), True Negative (TN), False Positive (FP) and False Negative (FN) pixels are used. These quantities are explained as follows:

TP: The number of pixels correctly identified as OD pixels; TN: The number of pixels correctly identified as non-OD (background) pixels; FP: The number of pixels of non-OD identified as OD pixels; FN: The number of pixels of OD pixels identified as non-OD pixels; The seven considered metrics are described and defined in (Eq. (21), ..., Eq. (27)).

1/Acc refers to the ratio of correctly segmented pixels in each class (OD and non-OD) to the total number of pixels in the image. It is the proportion of pixels that are correctly classified;

$S_{2/DC}$ is the similarity measure between segmented and annotated ODs;

$\frac{1}{2}JC$ is also called the Jaccard index, the OD area overlap or the intersection over union. It denotes the ratio of intersecting area of the segmented OD and the ground-truth to the union area of the segmented OD and the ground-truth of the OD. It is a similarity measure allowing to identify which pixels are shared and which are distinct:

$4/\Pr$ describes the correctness of the segmented region. It is expressed as the ratio of correctly segmented OD pixels to all the

segmented OD pixels. It is the proportion of pixels segmented as OD pixels that are OD pixels in the annotated image; $5/Se$ is also known as Recall or TP fraction. It denotes the ratio of correctly segmented OD pixels to the number of OD pixels annotated in the ground-truth. It estimates the success rate of achieving the annotated OD region. It is the proportion of the pixels in the OD region estimated as OD pixel:

$$Acc = \frac{TP + TN}{TP + TN + FP + FN} \quad (21)$$

$$DC = \frac{2 \times TP}{2 \times TP + FN + FP} \quad (22)$$

$$JC = \frac{TP}{TP + FN + FP} \quad (23)$$

$$Pr = \frac{TP}{TP + FP} \quad (24)$$

$$Se = \frac{TP}{TP + FN} \quad (25)$$

$$Sp = \frac{TN}{TN + FP} \quad (26)$$

$$Fs = 2 \times \frac{Pr \times Se}{Pr + Se} \quad (27)$$

It can be noticed that a higher value of Acc, Se, Sp, F-score, JC and Pr denotes a better segmentation result, and the metric DC must be close to 1 to attain a perfect segmentation result.

4.2. Database description

In this work, 10 different publicly available databases and one local database are used for evaluating our proposed method, compared to the current state of the art methods. These public databases are CHASE DB [86], Drive [87], High-Resolution Fundus (HRF) images database [88], Drishti-GS [80,89], Digital Retinal Images for Optic Nerve Segmentation (DRIONS) [90], Retinal Image Database for Optic Nerve Evaluation (RIM-ONE) [91], Indian Diabetic Retinopathy Images Dataset (IDRID) [92] and Retinal fundus Images for Glaucoma Analysis (RIGA) [93] composed of Bin Rushed, Magrabi, and Messidor sub-datasets.

The local database contains 220 fundus retinal images kept from 568 images of 173 patients affected by DR. These images are obtained from Fatouma Bourguiba Hospital, Monastir, Tunisia. These images are de-identified and are with no patient related data. They were produced without any constraint concerning the contrast or brightness and with a variety of shooting positions and they were taken between 2014 and 2020.

Each of Chase, Drive and local databases was manually delimited by a specialist ophthalmologist. In the HRF Database, the center point and radius of the OD were detected by an expert. Segmentation soft map is used to annotate the OD in Drishti database. In Drions database 36 points' coordinates of OD are used as a ground-truth. The OD in Rim-One database was annotated through a proposed software. Finally, in Riga dataset a manual marking was used in the annotation of OD in fundus image.

Table 2 shows a summary of the number of images, the type of the acquisition device, the angle of FOV, the image resolution, the eye diseases of patients, the position of acquired images, the number of expert annotations and the country of origin, for each of the databases. **Fig. 12** presents an example of retinal fundus image in each used database.

Table 2

Summary of the used databases of retinal fundus images; with 'H': healthy, 'UH': unhealthy, 'G': Glaucoma, 'GS': Glaucoma Suspects, 'DR' Diabetic Retinopathy' and 'M': Macula, 'ONH': Optic Nerve Hypoplasia.

Dataset	Number of images	Acquisition device	Fov (°)	Resolution (pixels)	Eye diseases	Centered around	Number of Experts	Annotation method	Country
Chase	28	Nidek NM-200-D fundus camera	30	999 × 960	H	ONH	1	Manual segmentation	England
Drive	40	Canon CR5	45	565 × 584	H	M	1	Manual segmentation	
HRF	45	Canon CF-60 non-mydiatic camera	60	3504 × 2336	15 H, 15 G, 15 DR	M	1	Center point and radius for OD	
Drishti	101		30	2049 × 1762	31 H, 70 UH	ONH	4	Segmentation Soft Map	India
Drions	110	Color analogical fundus camera		600 × 400	110 G	ONH	2	36 points' coordinates of OD	Spain
Rim One	159	Nidek AFC-210 Canon EOS 5D Mark II of 21.1 megapixels	30	1072 × 1424	85 H, 39 G, 35 GS	ONH	2	Manual segmentation	Spain
IDRID	597	Kowa VX-10 alpha digital fundus camera	50	4288 × 2848	597 DR	M	1	Pixel level annotation	India
Bin Rushed	195	Canon CR2 non-mydiatic		2376 × 1584	195 G	ONH, M	6	Manual marking	Saudi Arabia
Magrabi	95	Topcon TRC 50DX		2743 × 1946	95 G	ONH, M	6	Manual marking	Saudi Arabia
Messidor	460	Topcon TRC NW6	45	2240 × 1488, 1440 × 960	460 G	M	6	Manual marking	
Local DB	220	Topcon TRC non-mydiatic retinography	20 to 55	2588 × 2277	220 DR	M	1	Manual segmentation	Tunisia

5. Results and discussion

In this section, we aim to discuss most of the parameter setting in the proposed algorithm. In addition, qualitative and quantitative results are presented to show the performance of both the OD localization and segmentation of the proposed algorithm.

5.1. Parameter setting

This paper presents a novel method to detect and segment the optic disc in retinal fundus images. A personal computer is used to perform this process, with "intel(R) Core (TM), 2.70 GHz" processor and 12 GB of Random-Access Memory as a configuration system. The proposed algorithm was testing on ten publicly available databases and a local database. It was implemented using MATLAB R2018b version.

Our algorithm was tested by adjusting the values of the hyper-parameters to match the ground-truth results. First, to localize the optic disc, a blood vessel masking step was utilized. In which, we have proposed a combination between the two obtained in-painted vessel images (*Eq. (11)* in Section 3.1.2.6). **Table 3** presents the variation of the weight coefficient α from 0 to 1 for all the used databases.

By analyzing **Table 3**, it is notable that the suitable value of α is 0.75.

Second, the geometric analysis using a specific feature determines the final decision of the proposed OD localization method. Thus, the selection of the appropriate feature is an important step. To do that, we experimentally study the impact of selecting the optic disc region by calculating the circularity (illustrated by *Eq. (12)*) and the eccentricity (defined by *Eq. (28)*).

$$Ecc = \frac{\sqrt{(M_j/2 - M_n/2)^2}}{M_n/2} \quad (28)$$

where; M_j is the major axis length, and M_n is the minor axis length of the region.

Table 4 illustrates the comparison of the accuracy rate of the proposed OD localization method using the minimum of eccentricity and the maximum of circularity to select the optic disc region.

The geometric analysis using the calculation of the circularity yields the best performance in all the used databases.

Furthermore, in all the steps of our proposed algorithm, there are

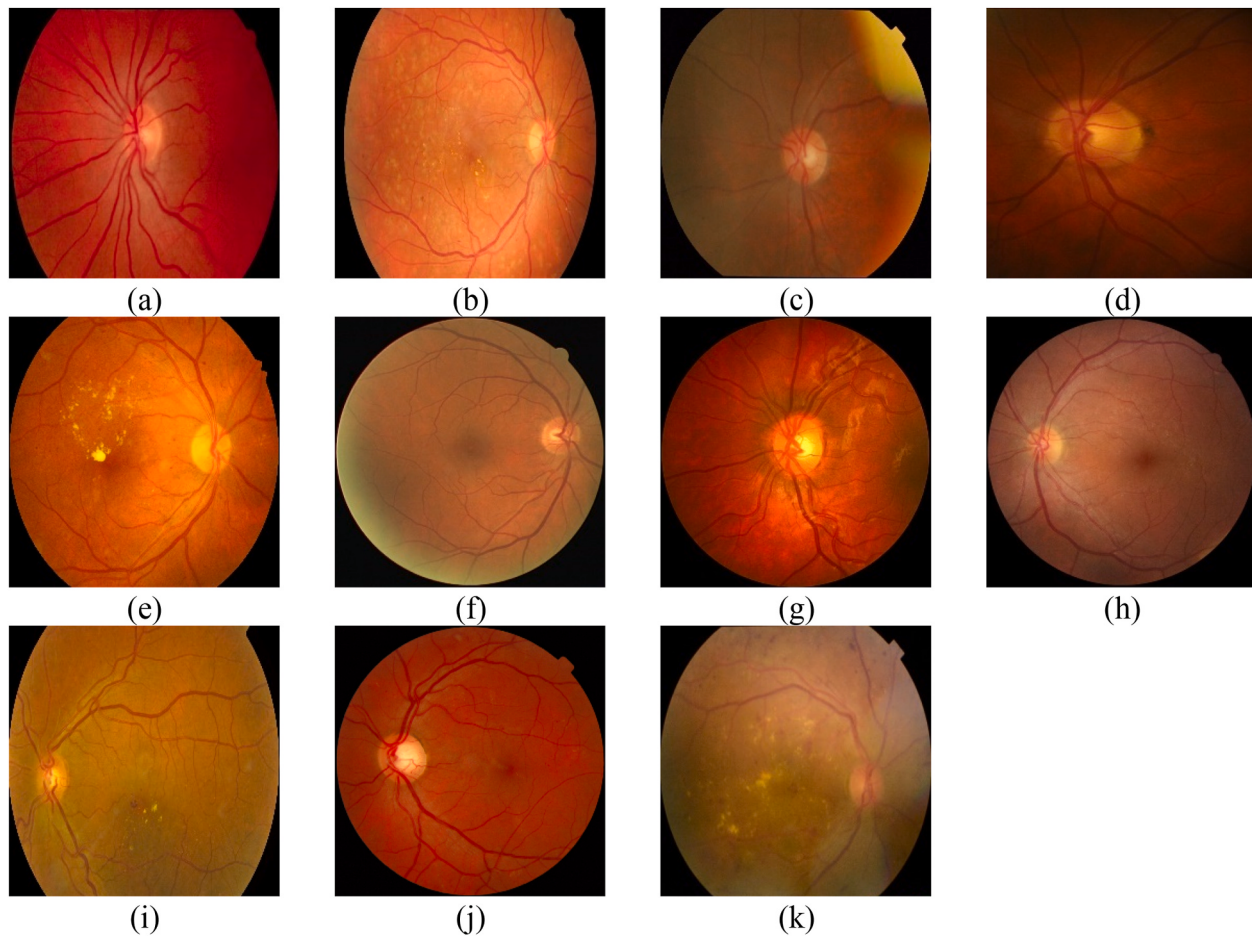


Fig. 12. Examples of fundus retinal images in each database: (a) Drions, (b) HRF, (c) Drishti, (d) Rim-One, (e) IDRID, (f) Drive, (g) Chase, (h) Bin Rushed, (i) Magrabi, (j) Messidor and (k) Local DB.

Table 3

Accuracy rate of the proposed OD localization method with α taking different values.

Database	Number of images	$\alpha = 0$	$\alpha = 0,25$	$\alpha = 0,5$	$\alpha = 0,75$	$\alpha = 1$
Chase	28	96,43	92,86	82,14	100	71,43
Drive	40	75,00	92,50	97,50	100	77,50
HRF	45	91,11	97,78	95,56	100	93,33
Drishti	101	76,24	94,06	98,02	100	99,01
Drions	110	88,18	98,18	99,09	100	98,18
Rim One	85	71,76	90,59	95,29	97,65	98,82
	74	79,73	91,89	91,89	98,65	94,59
IDRID	81	75,31	85,19	97,53	100	93,83
	516	95,74	98,26	99,22	99,42	99,42
Bin	50	80,00	88,00	98,00	100	96,00
Rushed	47	68,09	80,85	89,36	100	95,74
	47	85,11	95,74	95,74	100	93,62
	51	92,16	94,12	90,20	100	98,04
Magrabi	48	64,58	77,08	89,58	100	100
	47	97,87	95,74	91,49	100	95,74
Messidor	460	99,35	98,26	98,70	100	99,78
Local DB	220	99,09	97,27	98,18	100	97,73

several hyper-parameters fixed after several tests. These parameters are grouped in the Table 5.

5.2. OD localization

To assess the generalization ability and the robustness of the proposed OD localization algorithm, a local database as well as 10 publicly

Table 4

Accuracy rate of the proposed OD localization method depending on the circularity and the eccentricity feature.

Database	Minimum eccentricity	Maximum circularity
Chase	89,29	100
Drive	72,50	100
HRF	100	100
Drishti	98,02	100
Drions	100	100
Rim One	97,65	98,82
	98,65	97,30
IDRID	93,83	100
	98,84	99,42
Bin Rushed	92,00	100
	100	100
	97,87	100
	100	100
Magrabi	100	100
	100	100
Messidor	99,57	100
Local DB	99,09	100

available databases, namely ChaseDB1, Drive, HRD, Drishti, Drions, Rim-One, IDRID, Bin Rushed, Magrabi and Messidor, are used. The total number of images in these databases is 2,050 retinal fundus images, with various resolutions, FOVs, color intensity, degrees of contrast and pathologies.

Table 6 presents the number of images correctly localized and the accuracy rate of the suggested method for each database. The mean of accuracy rate for all databases is 99.8%, which means only 6 images out

Table 5
Parameters setting.

Parameter	Value
Number of tiles in CLAHE method	8
Contrast improvement limit in CLAHE method	0.01
Standard deviation of Gaussian filter	4
Length of the linear structuring element in the morphological operations step	150
Angle of the linear structuring element in the morphological operations step	0, 45, ..., 315
Window size of Bernsen thresholding	[25,25]
Weight coefficient of the vessel inpainting equation	0.75
Angle of the line orientation of the supremum of opening	10
β in the range of the major axis length of the roi	0.66

of 2,050 images are considered as incorrectly localized. Specifically, the proposed algorithm successfully localizes 156 images out of 159 images in the Rim-One database and 594 images out of 597 images in the IDRID database. On the other hand, all the images in the Drions, HRF, Drishti, IDRID, Chase, Drive, Bin Rushed, Magrabi, Messidor databases and the local database are correctly localized.

It should be noted that the few cases of non-localized OD images are caused by the bad quality of the retinal image such as the blurred images, as illustrated in Fig. 13(a). We can also mention the failure in locating the OD in the fundus image with severe peripapillary atrophies, which cover in a complete way the OD, as despite in Fig. 13(b). Besides

the existence of these atrophies, the detected OD centroid is very close to the OD region.

Nevertheless, the proposed method successfully localizes the OD on several challenging cases, for instance the images cited in Fig. 14. The OD in Fig. 14(a–c) lacks the brightness characteristic. Images in Fig. 14 (d–f) have poor quality where the vessels are uncertain, and the OD is not well defined. In Fig. 14 (g), the OD is not visible. Despite that, the OD is well defined in a blurred image, as shown in Fig. 14(h–i). Moreover, in Fig. 14 (j) the OD is well localized even with retinal thickness showing the presence of peripapillary atrophies which are more sizeable than the OD.

In addition, comparing the localization results of different literature methods on the same datasets used in our work, is presented in Table 6. As it can be noticed, most of state-of-the-art methods have not been evaluated on the 10 publicly databases. Besides, the localization accuracy of the suggested algorithm is over the rate of 98.06% for all the databases and with a mean accuracy rate equal to 99.80%, which makes our proposed algorithm very attractive compared to its counterparts. Compared with the works of Almazroa et al. [28], Chalakkal, et al. [43], Almubarak et al. [29] and Bhatkalkar et al. [26], the highest detection rate is obtained by the proposed algorithm on the Rim-One, IDRID, Bin Rushed and Messidor databases with 98.06%, 99.71%, 100% and 100%, respectively. The work of Latif et al. [51] presents a higher accuracy rate on Rim-One database in comparison with our result. However, our algorithm performs better with DRIVE and DRIONS databases with 100%

Table 6
Comparison of OD detection methods in state-of-the-art for Chase, Drive, HRF, Drishti, Drions, Rim-One, IDRID, Bin Rushed, Magrabi, Messidor and Local databases.

	Chase	Drive	HRF	Drishti	Drions	Rim One	IDRID	Bin Rushed	Magrabi	Messidor	Local DB
Total image	28	40	45	101	110	159	597	195	95	460	220
Muhammed et al. [23]	75	95	–	–	77	–	–	–	–	–	–
Reza et al. [38]	–	97.5	–	97.03	100	–	–	–	–	–	–
Chalakkal et al. [15]	100	100	–	–	–	–	96.12	–	–	–	–
Guo et al. [25]	96.43	97.5	97.78	–	100	–	–	–	–	–	–
Ramani et al. [34]	100	100	100	100	100	–	–	–	–	–	–
Bhatkalkar et al. [26]	–	–	–	–	–	96.43	–	–	–	–	–
Almazoa et al. [28]	–	–	–	–	–	–	–	87.6	89.8	–	–
Almubarak et al. [29]	–	–	–	–	–	–	–	–	100	98.04	–
Escorcia et al. (GC) [64]	–	100	97.7	–	–	–	–	–	–	–	–
Escorcia et al. (EMT + HT) [64]	–	95	95.5	–	–	–	–	–	–	–	–
Khaing et al. [63]	–	–	100	100	–	–	–	–	–	–	–
Al Shalchi et al. [44]	–	100	–	–	–	–	–	–	–	–	–
[Kaya et al. [42]]	–	97.5	–	–	100	–	–	–	–	–	–
Ali et al. [39]	–	100	100	–	–	–	–	–	–	–	–
Kumar et al. [45]	100	97.5	–	–	100	–	–	–	–	–	–
Latif et al. [51]	–	–	98.05	–	98.83	99.05	–	–	–	–	–
Khan et al. [35]	–	–	–	–	100	–	–	–	–	–	–
Proposed Method	100	100	100	100	100	98.06	99.71	100	100	100	100



(a)



(b)

Fig. 13. Examples of results of OD localization method with incorrectly localized OD: (a) blurred image, (b) image with large bright peripapillary region, with green dot indicating centroid of detected OD.

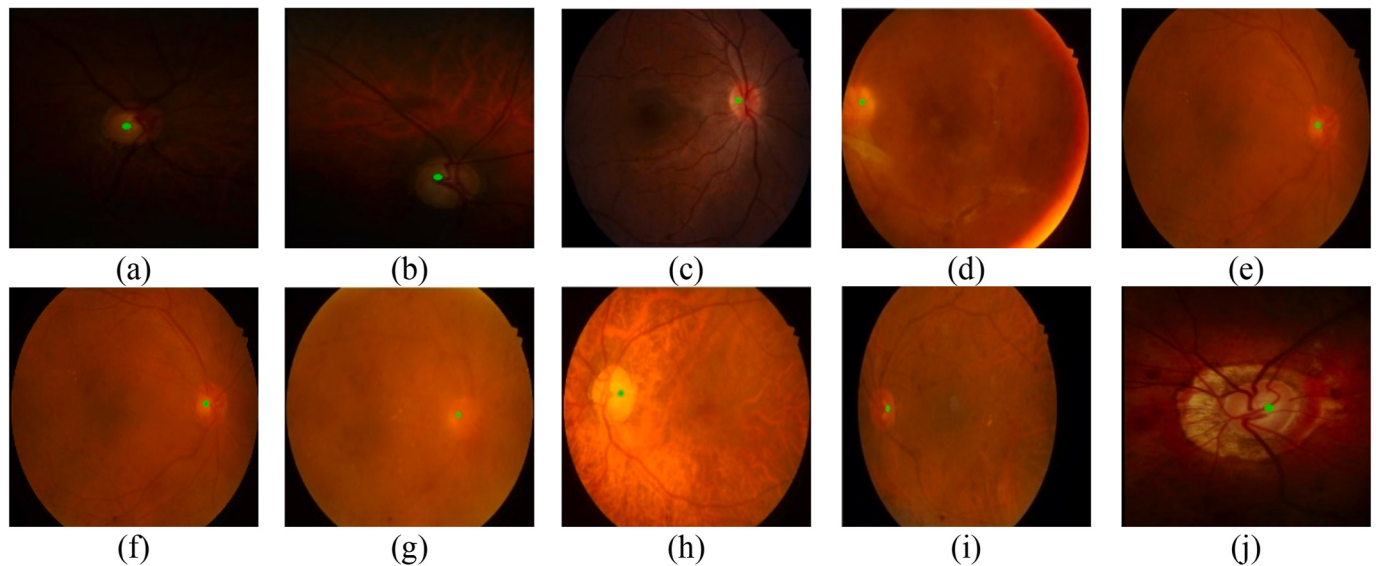


Fig. 14. Examples of results of OD Localization method with ODs successfully localized in different databases, with green dot representing detected OD centroid.

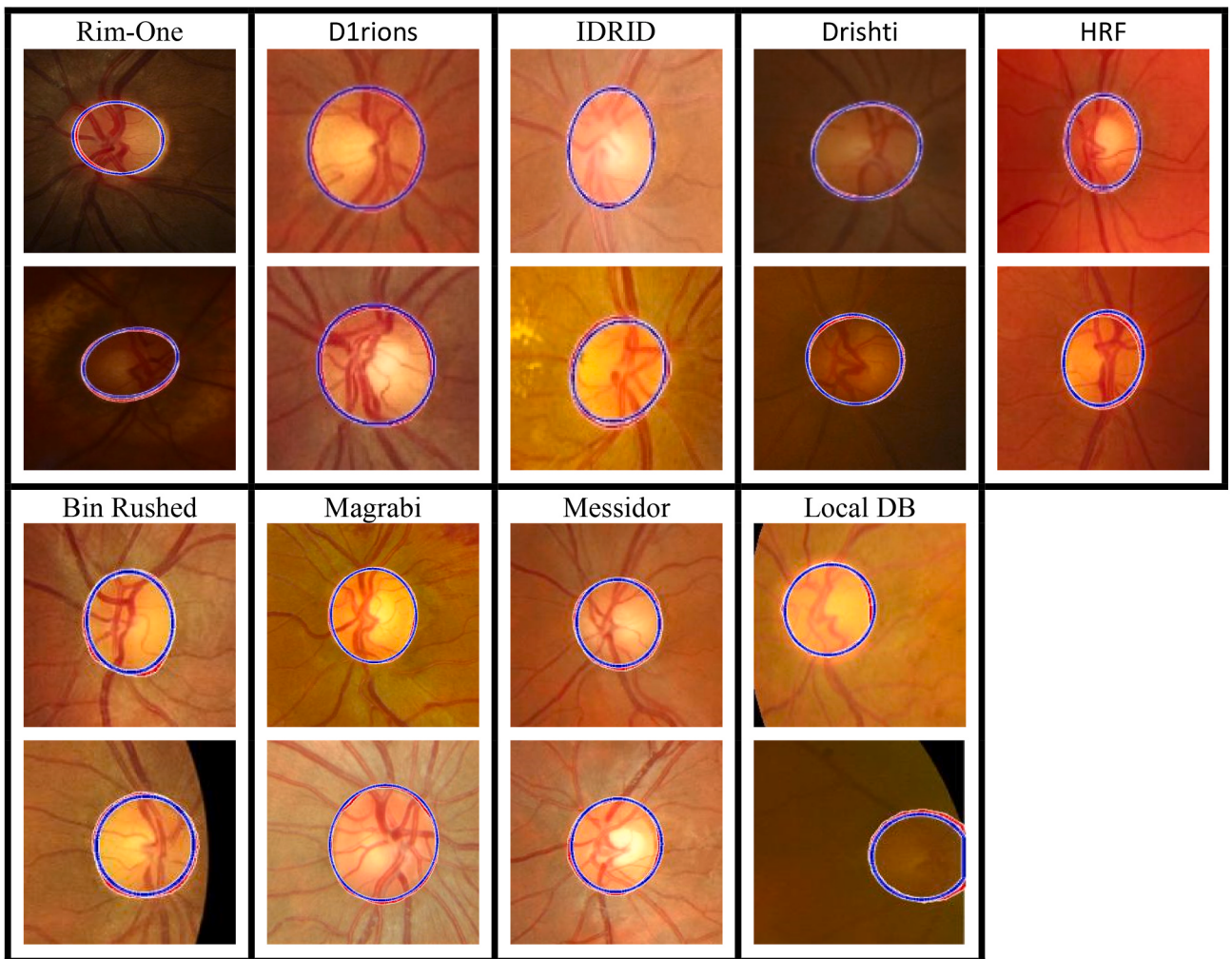


Fig. 15. Examples of results of the proposed OD segmentation algorithm in each database. Blue: OD segmentation result overlaid on original image, red: Ground-truth overlaid on original image.

accuracy rate. In addition, our method was tested on 2,050 images whereas Latif's et al. implemented the proposed approach in only 958 images. Compared to other studies such as [23–25,34,38,63,64], our proposed algorithm is similar or even better for the Chase, Drive, HRF, Drishti, Drions and Magrabi databases with a 100% OD localization rate.

5.3. OD segmentation

In this section, we focus on the qualitative and quantitative results for OD segmentation method on Rim One, Drions, IDRID, Drishti, HRF, Bin Rushed, Magrabi, Messidor databases and a local database. Fig. 15 illustrates some examples for the OD segmentation results with ground-truth marking in which the segmented contour (in blue) and the ground-truth contour (represented in red) of the optic disc are superposed on the colored original image.

The quantitative evaluation of the proposed methodology in term of JC and DC coefficients is presented in Table 7. The evaluation is performed in terms of percentage of images per Jaccard coefficient intervals ($JC > 0.9$, $JC > 0.8$, $JC > 0.7$, $JC > 0.6$ and $JC > 0.5$) and Dice coefficient intervals (the same JC intervals). In addition, the JC average represented by \bar{JC} as well as the DC average which represented by \bar{DC} for diverse datasets (Drions, IDRID, RimOne, HRF, Drishti, Bin Rushed, Magrabi, Messidor and Local DB) are shown in the last column of Table 7.

These values prove the stability and the robustness of the proposed OD segmentation method for different datasets.

Fig. 16 indicates the comprehensive OD segmentation performance results of our method upon nine databases calculated in terms of Acc, Se, Sp and DC represented by the box-whisker diagram. This diagram shows the distribution and variability of values in groups.

The experimental results show the evaluation of the metrics in each dataset. It can be witnessed that the median values, represented by the horizontal central line in each box, are around 99.7%; 97.98%; 99.77% and 92.07% in terms of accuracy, sensitivity, specificity and dice coefficient, respectively, as mentioned in Table 8.

Besides the qualitative and quantitative evaluation, it is important to compare the proposed OD segmentation method with the-state-of-the-art methods in terms of performance metrics described in Section 5. Table 9 compares the proposed method with different state-of-the-art approaches including traditional, supervised and unsupervised methods.

As can be observed, the results obtained by the proposed approach outperform those of the literature methods for most evaluation metrics for the IDRID database (Table 9). Using the DL architecture with few

training images, Hasan et al. [61] correctly labeled 89.9% pixels for the IDRID dataset, whereas it is 96.92% for our proposed approach. The sensitivity of the suggested method for the HRF, Drishti, IDRID and RimOne databases is quite promising compared to the literature methods. On the other hand, Pathan, et al. [19] outperformed our method in terms of sensitivity, using the decision tree classifier which was tested on only one public database (Rim One) with low specificity and accuracy.

The proposed system consistently achieves comparable or better results in terms of sensitivity when compared to the literature methods that tested the Drions database, except for Rehman et al. [18] and Khan et al. [35] who obtained lower specificity, accuracy, and Dice coefficient values. In addition, Khan et al. [35] got lower accuracy (99.60%) and sensitivity (96.49%) for the Drishti database by comparing with our method which has an accuracy of 99.62% and a sensitivity of 98.20%. These rates are quite high when compared to Diaz-Pinto et al. [49] with 75.25% and 74.19% for accuracy and sensitivity, respectively.

The proposed approach also yields the highest accuracy with 99.62% and 99.37% for the Drishti and Rim One databases, respectively. It is noticeable that the accuracy of our suggested system (99.61%), gets closer to the best results for the HRF database obtained by Ramani et al. [34] with 99.67%. More specifically, a weak performance of Ramani et al. [34] in terms of sensitivity for the Drions and HRF databases were produced with 92.3% and 84.56%, respectively, while our method obtains 92.66%. Moreover, for Drions database, Abdullah et al. [43] and Nija et al. [36] obtained a lower sensitivity value with 88.63% and 90.71%, respectively, contrary to our system (94.24%). Our Dice coefficient is higher than the methods of Ramani et al. [34] and Rehman et al. [18] for the Drions and Drishti databases. Furthermore, our method outperforms Ramani et al. [34], Rehman et al. [18] and Escorcia et al. [64] for Drions, HRF and Drishti databases, respectively, in terms of OD overlap. Moreover, the precision and the F-score of the suggested method is quite competitive compared to Khaing et al. [63]. These two metrics have not been mentioned in all the above cited literature methods.

By analyzing the obtained values of the Dice coefficient metric, we notice that the proposed approach outperforms all the cited state-of-the-art methods on all the tested datasets except RimOne dataset. In addition, the proposed OD segmentation method outperforms the literature methods, according to our knowledge, for Drions, Drishti, Bin Rushed and Magrabi datasets. In the HRF dataset, the proposed method surpasses the Ramani et al. [34], Zahoor et al. [13] and the EMT and HT-based method of Escorcia et al. [64], in terms of Jaccard index of.

Table 7
The JC and DC results of the proposed OD segmentation method.

		$JC > // DC >$					$\bar{JC} // \bar{DC}$
		0.90	0.80	0.70	0.60	0.50	
Drions	JC	23.64%	70.91%	90.00%	92.73%	95.45%	90.00%
	DC	68.18%	90.00%	95.45%	97.27%	97.27%	93.86%
IDRID	JC	27.16%	61.73%	76.54%	86.42%	90.12%	81.23% 87.35%
	DC	58.02%	82.72%	87.65%	92.59%	95.06%	
RimOne	JC	1.18%	27.06%	55.29%	74.12%	87.06%	65.41%
	DC	21.18%	61.18%	80.00%	94.12%	96.47%	77.35%
HRF	JC	26.67%	60.00%	84.44%	88.89%	97.78%	87.11% 91.11%
	DC	42.22%	84.44%	93.33%	95.56%	100%	
Drishti	JC	53.47%	87.13%	94.06%	99.01%	99.01%	96.44%
	DC	94.06%	98.02%	100%	100%	100%	99.50%
Bin Rushed	JC	34.87%	89.74%	98.97%	99.49%	100%	98.87%
	DC	97.44%	98.97%	100%	100%	100%	99.62%
Magrabi	JC	51.58%	92.63%	97.89%	97.89%	98.95%	97.89%
	DC	96.84%	97.89%	97.89%	98.95%	100%	98.16%
Messidor	JC	37.61%	81.30%	90.22%	92.17%	93.26%	90.87%
	DC	88.26%	91.09%	93.04%	94.35%	96.96%	92.66%
Local DB	JC	46.61%	78.28%	90.50%	95.48%	97.74%	92.76%
	DC	87.78%	93.67%	97.29%	98.19%	98.64%	96.15%
Total (2,050 images)		33.64%	72.09%	86.44%	92.29%	95.49%	88.95%
		67.02%	88.66%	93.85%	96.78%	98.27%	92.86%

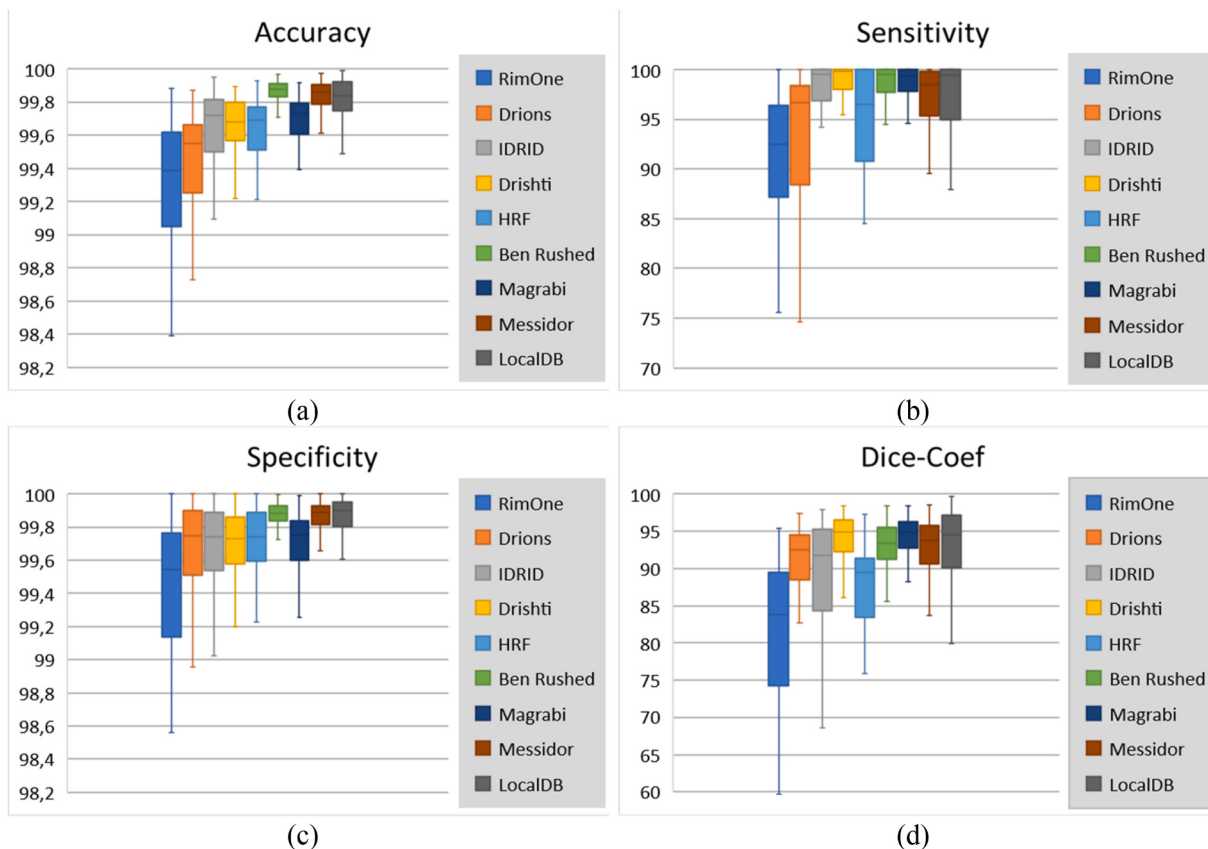


Fig. 16. Box-whisker of OD segmentation performances on nine databases; (a) accuracy, (b) sensitivity, (c) specificity and (d) dice coefficient.

Table 8
Median of performances of OD segmentation in all databases.

	Accuracy (%)	Sensitivity (%)	Specificity (%)
Rim One	99.39	92.49	99.55
Drions	99.55	96.65	99.75
IDRID	99.72	99.51	99.74
Drishti	99.68	99.81	99.73
HRF	99.69	96.47	99.74
Bin Rushed	99.88	99.59	99.88
Magrabi	99.73	99.34	99.75
Messidor	99.86	98.54	99.89
Local DB	99.84	99.44	99.90
Median value	99.7	97.98	99.77

Although, our obtained Jaccard index value is close to the one of the GC-based method of Escorcia et al. [64]. It should be mentioned that the proposed method outperforms the previous cited method in terms of accuracy, sensitivity and specificity.

Furthermore, as given in Table 9, the proposed method surpasses the method of Kim et al. [31] in terms of sensitivity, specificity and accuracy for all the datasets of Riga (Bin Rushed, Magrabi and Messidor) except the Messidor database where the resulting sensitivity is very close to the results of Kim et al. [31]. The mean accuracy, sensitivity, specificity and Jaccard index are 99.80%, 98.19%, 99.83% and 95.87%, respectively, for all the datasets of Riga. However, the mean of previous metrics of Kim et al. [31] are 99.07%, 97.58%, 99.41% and 95%, respectively, which demonstrates the power of the proposed method compared to the other algorithms.

Table 10 shows a comparison between the performance of the proposed algorithm of the OD segmentation and the state-of-the-art methods that have used the RIGA database. The mean and the median values of different metrics (Accuracy, Sensitivity, Specificity, Dice

Coefficient and the Jaccard Coefficient) for OD segmentation on RIGA database are presented in this table. It is noteworthy that our algorithm has the highest in terms of all the above-mentioned metrics compared to Kim et al. [31], Shi et al. [62] and Carvalho et al. [54] methods.

The overall results of the proposed method show to which extent the presented OD segmentation method is comparable to the literature methods for both healthy and diseased samples with DR or glaucomatous fundus retinal images with various qualities, which makes our approach more robust and quite competitive in comparison to the existing methods.

By analyzing our method, it is clear that the major advantage is the use of simple methods which can lead to the usage of our algorithm without a large processor. Besides, the proposed algorithm is implemented on a large number of retinal fundus images and large datasets containing variety of images. But unfortunately, a relatively large time is needed to segment the retinal image which reaches 30s. However, this is still applicable and not very big enough. Also, the step to segment the optic disc is the major disadvantage associated with our method which may increase the dependency on the vessel extraction processing time.

6. Conclusion and future work

The OD localization and segmentation are very challenging tasks due to the diverse artifacts and image variability. In this paper, we proposed a novel method of optic disc segmentation. The main phases of our proposed approach are: the vascular structure inpainting, the OD detection and finally the OD segmentation. The efficiency of the suggested algorithm is improved by numerical evaluation parameters as compared with other literature methods. Considering the direction and width of blood vessels, the proposed algorithm manages to exclude the vascular structure using the Bernsen thresholding. A saliency map is proposed in this paper to highlight the bright regions wielding the

Table 9

OD segmentation performance values with comparison of state-of-the-art methods; The highest value is in blue and the predecessor is in red.

Method	Acc	Se	Sp	\overline{DC}	\overline{JC}	Pr	Fs
Drions							
Ramani et al. [34]	99.37	92.49	99.59	89.62	82.17	–	–
Morales et al. [7]	99.34	–	–	90.84	–	–	–
Abdullah et al. [47]	95.49	85.08	99.66	91.02	85.10	–	–
Naqvi et al. [17]	96.72	91.30	98.00	–	84.31	–	–
Rehman et al. [17]	99.30	96.90	99.40	89.90	82.10	–	–
Fan et al. [16]	97.60	89.57	–	91.37	84.73	–	–
Khan et al. [35]	99.31	94.41	99.56	–	85.89	–	–
Nija et al. [36]	99.89	90.71	99.66	–	88.80	–	–
Abdullah et al. [43]	99.42	88.63	99.56	–	84.31	–	–
Kim et al. [41]	98.94	91.08	99.21	–	–	–	–
Wang et al. [57]	96.00	92.40	–	–	–	–	–
Kumar et al. [45]	99.14	86.68	99.54	–	–	–	–
Latif et al. [51]	93.25	92.85	93.80	–	–	–	–
Proposed method	99.41	92.66	99.64	93.86	90.00	89.00	90.12
HRF							
Ramani et al. [34]	99.67	84.56	99.87	87.13	79.41	–	–
Zahoor et al. [13]	97.74	92.33	98.92	–	86.86	–	–
Escorcia et al. (GC) [64]	98.80	93.90	–	–	87.72	–	–
Escorcia et al. (EMT + HT) [64]	86.50	74.40	–	–	45.93	–	–
Diaz-Pinto et al. [49]	80.00	83.30	–	–	–	–	–
Abdel-Hamid et al. [30]	96.70	93.30	100	–	–	–	–
Shanthamalar et al. [14]	95.67	–	98.33	–	–	–	–
Latif et al. [51]	92.25	91.75	91.30	–	–	–	–
Proposed method	99.61	94.24	99.70	91.11	87.11	80.84	86.21
Drishti							
Ramani et al. [34]	99.22	94.95	99.34	86.63	77.80	–	–
Khan et al. [35]	99.60	96.49	99.75	–	91.79	–	–
Al-Bander et al. [48]	97.76	94.88	99.93	96.38	93.01	–	96.38
Naqvi et al. [17]	–	97.54	99.73	95.97	91.83	–	–
Chalakkal et al. [15]	–	97.59	99.90	96.42	93.23	–	–
Khaing et al. (ADI-GVF) [63]	–	78.97	–	–	–	84.35	81.10
Khaing et al. (RG) [63]	–	59.39	–	–	–	91.98	72.18
Khaing et al. (GVF) [63]	–	89.81	–	–	–	60.51	72.31
Diaz-Pinto et al. [49]	75.25	74.19	71.43	–	–	–	–
Joshi et al. [50]	–	–	–	97.00	96.00	–	–
Hervella et al. [55]	–	–	–	97.18	–	–	–
Yi et al. [40]	92.82	85.00	99.00	84.15	90.20	–	–
Xiong et al. [56]	99.70	98.31	99.74	94.36	89.51	–	–
Yu et al. [53]	98.41	–	–	97.39	–	–	–
Proposed method	99.62	98.20	99.66	99.50	96.44	89.93	93.57
Rim One							
Pathan et al. [19]	99.16	93.91	99.40	90.70	85.30	–	–
Al-Bander et al. [48]	99.22	87.37	99.76	90.36	82.89	–	–
Lu et al. [60]	99.32	90.38	99.94	–	89.58	–	–
Abdullah et al. [47]	99.89	85.08	99.66	–	85.10	–	–
Diaz-Pinto et al. [49]	71.21	79.31	79.90	–	–	–	–
Yi et al. [40]	94.31	90.00	98.00	89.85	–	–	–
Xiong et al. [56]	99.16	97.35	99.23	87.56	78.31	–	–
Khan et al. [35]	99.09	96.11	99.32	–	85.68	–	–
Proposed method	99.31	90.48	99.44	77.35	65.41	74.02	80.30
IDRID							
Saha et al. [52]	98.29	–	–	–	96.44	–	–
Hasan et al. [61]	99.70	89.90	–	–	84.50	–	–
Chalakkal et al. [15]	–	96.60	–	–	85.60	–	–
Proposed method	99.62	96.92	99.66	87.35	81.23	81.32	87.32
Bin Rushed							
Kim et al. [31]	99.02	96.53	99.59	–	94.78	98.16	97.30
Proposed method	99.87	98.47	99.87	99.62	98.87	88.14	92.86
Magrabi							
Kim et al. [31]	99.07	98.52	99.20	–	94.95	96.36	97.41
Proposed method	99.69	98.56	99.72	98.16	97.89	89.44	93.54
Messidor							
Kim et al. [31]	99.12	97.70	99.44	–	95.27	97.49	97.57
Proposed method	99.79	96.32	99.83	92.66	90.87	85.84	89.95
Local DB							
Proposed method	99.77	96.03	99.82	92.86	88.95	89.64	92.50

supremum of opening and the regional maxima which are able to segment the OD automatically without specifying the threshold value.

The proposed OD segmentation method is robust even for images having peripapillary atrophies, exudates, cotton wool and artifacts. The addressed challenges regarding OD segmentation are:

- The OD localization, which is the most important step, achieves 100% of accuracy for the used databases except Rim One and IDRID, with a high mean accuracy of 99.8%;

Table 10

OD segmentation performance values with comparison of state-of-the-art methods that have used the RIGA database; Bold-font denotes the best metrics.

	Acc	Se	Sp	DC	JC
	Mean (Median)	Mean (Median)	Mean (Median)	Mean (Median)	Mean (Median)
Kim et al. [31]	99.07	97.58	99.41	–	95
Shi et al. [62]	–	95.39 (96.72)	–	95.57 (96.46)	91.67 (93.16)
Carvalho et al. [54]	–	–	–	94.34	–
Proposed method	99.75 (99.79)	97.78 (98.47)	99.81 (99.83)	96.81 (98.16)	95.88 (97.89)

- The average accuracy of OD segmentation on the used datasets (the Rim One, Drions, IDRID, Drishti, HRF, Bin Rushed, Magrabi, Messidor and LocalDB databases) is about 99.63%;
- The mean specificity of OD segmentation on the above-mentioned datasets reaches 99.70%;
- The evaluation of the proposed method shows the stability and the robustness of the system with overall accuracy, specificity and sensitivity, which are very high compared to the recent works in the state of the art;
- The number of fundus retinal images used to evaluate our approach is about 2,050 images, which is a large database composed of 11 different datasets;
- The use of information from more than one channel has led to enhance the precision of our method.

The robustness of our approach compared to literature methods is explained by its performance in optic disc localization and its precision in optic disc segmentation for healthy and diseased samples with diabetic retinopathy or glaucomatous fundus retinal images with various qualities. The main advantage of the proposed approach is the use of simple methods. Moreover, our algorithm is evaluated on different large datasets of retinal fundus images.

As a future work, we aim to minimize the processing time of our algorithm by removing the vessel extraction step. Besides, we plan to diagnosis the glaucoma disease through the calculation of the cup-to-disc ratio by bringing out the features of the OD. In addition, this approach can be effective for detecting DR lesions.

Funding

This research did not receive any specific grant from funding agencies in the public, commercial, or not-for-profit sectors.

Declaration of competing interest

The authors whose names are listed immediately below certify that they have NO affiliations with or involvement in any organization or entity with any financial interest (such as honoraria; educational grants; participation in speakers' bureaus; membership, employment, consultancies, stock ownership, or other equity interest; and expert testimony or patent-licensing arrangements), or non-financial interest (such as personal or professional relationships, affiliations, knowledge or beliefs) in the subject matter or materials discussed in this manuscript.

Acknowledgement

Authors would like to extend my sincere thanks to Dr. Imen Khairallah Ksiaa Department of Ophthalmology, Fattouma Bourguiba University Hospital, Faculty of Medicine, University of Monastir, Tunisia for her help in the generation of the features annotation, we are also grateful to the Professor and Chairman Department of Ophthalmology Moncef

Khairallah, in Fattouma Bourguiba University Hospital, Faculty of Medicine and University of Monastir, Tunisia.

References

- [1] O. Mondiale de la Santé, Rapport mondial sur la vision, 2020.
- [2] L. Guariguata, D.R. Whiting, I. Hambleton, J. Beagleby, U. Linnenkamp, J.E. Shaw, Global estimates of diabetes prevalence for 2013 and projections for 2035, *Diabetes Res. Clin. Pract.* 103 (2) (2014) 137–149, <https://doi.org/10.1016/j.diabres.2013.11.002>.
- [3] T.A. Soomro, M.A. Khan, J. Gao, T.M. Khan, M. Paul, Contrast normalization steps for increased sensitivity of a retinal image segmentation method, *Signal Image Video Process.* 11 (8) (2017) 1509–1517, <https://doi.org/10.1007/s11760-017-1114-7>.
- [4] M. Niemeijer, M.D. Abramoff, B. van Ginneken, Image structure clustering for image quality verification of color retina images in diabetic retinopathy screening, *Med. Image Anal.* 10 (6) (2006) 888–898, <https://doi.org/10.1016/j.media.2006.09.006>.
- [5] N. Zaaboub, A. Douik, Early diagnosis of diabetic retinopathy using random forest algorithm, in: 2020 5th International Conference on Advanced Technologies for Signal and Image Processing (ATSiP), IEEE, 2020, September, pp. 1–5.
- [6] N. Zaaboub, A. Douik, Application of learning algorithm for diabetic retinopathy diagnosis, in: 2020 17th International Multi-Conference on Systems, Signals & Devices (SSD), IEEE, 2020, July, pp. 17–21.
- [7] S. Morales, V. Naranjo, J. Angulo, M. Alcañiz, Automatic detection of optic disc based on PCA and mathematical morphology, *IEEE Trans. Med. Imag.* 32 (4) (2013) 786–796, <https://doi.org/10.1109/TMI.2013.2238244>.
- [8] A. Almazroa, R. Burman, K. Raahemifar, V. Lakshminarayanan, Optic disc and optic cup segmentation methodologies for glaucoma image detection: a survey, *J. Ophthalmol.* (2015), <https://doi.org/10.1155/2015/180972>, 2015.
- [9] A. Allam, A. Youssif, A. Ghalwash, Automatic segmentation of optic disc in eye fundus images: a survey, *ELCVIA - Electron. Lett. Comput. Vis. Image Anal.* 14 (1) (2015) 1–20.
- [10] M.T. Mahmood, I.H. Lee, Optic disc localization in fundus images through accumulated directional and radial blur analysis, *Comput. Med. Imag. Graph.* 98 (2022), 102058.
- [11] T.T. Khaing, P. Aimmanee, S. Makhanov, H. Haneishi, Vessel-based hybrid optic disk segmentation applied to mobile phone camera retinal images, *Med. Biol. Eng. Comput.* 60 (2) (2022) 421–437.
- [12] F. Guo, H. Peng, B. Zou, R. Zhao, X. Liu, Localisation and segmentation of optic disc with the fractional-order Darwinian particle swarm optimisation algorithm, *IET Image Process.* 12 (8) (2018) 1303–1312, <https://doi.org/10.1049/iet-ipr.2017.1149>.
- [13] M.N. Zahoor, M.M. Fraz, Fast optic disc segmentation in retina using polar transform, *IEEE Access* 5 (2017) 12293–12300, <https://doi.org/10.1109/ACCESS.2017.2723320>.
- [14] J.J. Shanthamalar, R.G. Ramani, Automatic blood vessel segmentation in retinal fundus images using image enhancement and dynamic gray-level thresholding, in: *Proceedings of International Conference on Computational Intelligence and Data Engineering*, Springer, Singapore, 2022, pp. 337–348.
- [15] R.J. Chalakkal, W.H. Abdulla, S.S. Thulaseedharan, Automatic detection and segmentation of optic disc and fovea in retinal images, *IET Image Process.* 12 (11) (2018) 2100–2110, <https://doi.org/10.1049/iet-ipr.2018.5666>.
- [16] Z. Fan, Y. Rong, X. Cai, J. Lu, W. Li, H. Lin, X. Chen, Optic disk detection in fundus image based on structured learning, *IEEE J. Biomed. Health Inf.* 22 (1) (2017) 224–234, <https://doi.org/10.1109/JBHI.2017.2723678>.
- [17] S.S. Naqvi, N. Fatima, T.M. Khan, Z.U. Rehman, M.A. Khan, Automatic optic disk detection and segmentation by variational active contour estimation in retinal fundus images, *Signal Image Video Process.* 13 (6) (2019) 1191–1198, <https://doi.org/10.1007/s11760-019-01463-y>.
- [18] Z.U. Rehman, S.S. Naqvi, T.M. Khan, M. Arsalan, M.A. Khan, M.A. Khalil, Multi-parametric optic disc segmentation using superpixel based feature classification, *Expert Syst. Appl.* 120 (2019) 461–473, <https://doi.org/10.1016/j.eswa.2018.12.008>.
- [19] S. Pathan, P. Kumar, R. Pai, S.V. Bhandary, Automated detection of optic disc contours in fundus images using decision tree classifier, *Biocybern. Biomed. Eng.* 40 (1) (2020) 52–64, <https://doi.org/10.1016/j.bbe.2019.11.003>.
- [20] W. Zaaboub, L. Tlig, M. Sayadi, B. Solaiman, Neural network-based system for automatic passport stamp classification, *Inf. Technol. Control* 49 (4) (2020) 583–607, <https://doi.org/10.5755/j01.itc.49.4.25919>.
- [21] W. Zaaboub, L. Tlig, M. Sayadi, B. Solaiman, Logo detection based on FCM clustering algorithm and texture features, in: *International Conference on Image and Signal Processing*, Springer, Cham, 2020, June, pp. 326–336, https://doi.org/10.1007/978-3-030-51935-3_35.
- [22] W. Zaaboub, Z.B. Dhiaf, Approach of texture signature determination—application to forest cover classification of high-resolution satellite image, in: 2014 6th International Conference of Soft Computing and Pattern Recognition (SoCPaR), IEEE, 2014, August, pp. 325–330, <https://doi.org/10.1109/SOCPar.2014.7008027>.
- [23] L.A. Muhammed, Localizing optic disc in retinal image automatically with entropy-based algorithm, *Int. J. Biomed. Imag.* (2018), <https://doi.org/10.1155/2018/2815163>, 2018.
- [24] T. Devasia, P. Jacob, T. Thomas, Automatic optic disc localization in color retinal fundus images, *Adv. Comput. Sci. Technol.* 11 (1) (2018) 1–13.

- [25] J. Guo, G. Azzopardi, C. Shi, N.M. Janssonius, N. Petkov, Automatic determination of vertical cup-to-disc ratio in retinal fundus images for glaucoma screening, IEEE Access 7 (2019) 8527–8541, <https://doi.org/10.1109/ACCESS.2018.2890544>.
- [26] B. Bhatkalkar, A. Joshi, S. Prabhu, S. Bhandary, Automated fundus image quality assessment and segmentation of optic disc using convolutional neural networks, Int. J. Electr. Comput. Eng. 10 (1) (2020), <https://doi.org/10.11591/ijece.v10i1.8p816-827>.
- [27] M. Wu, T. Leng, L.D. Sisterne, D.L. Rubin, Q. Chen, Segmentation of Optic Disc and Cup-to-Disc Ratio Quantification Based on OCT Scans. Retinal Optical Coherence Tomography Image Analysis, Springer, Singapore, 2019, pp. 193–209.
- [28] A. Almazroa, A Novel Automatic Optic Disc and Cup Image Segmentation System for Diagnosing Glaucoma Using Riga Dataset, 2016.
- [29] H. Almubarak, Y. Bazi, N. Alajlan, Two-stage mask-rnn approach for detecting and segmenting the optic nerve head, optic disc, and optic cup in fundus images, Appl. Sci. 10 (11) (2020) 3833, <https://doi.org/10.3390/app10113833>.
- [30] L. Abdel-Hamid, Glaucoma detection from retinal images using statistical and textural wavelet features, J. Digit. Imag. 33 (1) (2020) 151–158, <https://doi.org/10.1007/s10278-019-00189-0>.
- [31] J. Kim, L. Tran, E.Y. Chew, S. Antani, Optic disc and cup segmentation for glaucoma characterization using deep learning, in: 2019 IEEE 32nd International Symposium on Computer-Based Medical Systems (CBMS), IEEE, 2019, June, pp. 489–494, <https://doi.org/10.1109/CBMS.2019.00100>.
- [32] L.K. Singh, H. Garg, M. Khanna, Performance evaluation of various deep learning based models for effective glaucoma evaluation using optical coherence tomography images, Multimed. Tool. Appl. (2022) 1–45, <https://doi.org/10.1007/s11042-022-12826-y>.
- [33] W. Li, W. Fang, J. Wang, Y. He, G. Deng, H. Ye, G. Shi, A weakly supervised deep learning approach for leakage detection in fluorescein angiography images, Transl. Vision Sci. Technol. 11 (3) (2022), <https://doi.org/10.1167/tvst.11.3.9>, 9–9.
- [34] R.G. Ramani, J.J. Shanthamalar, Improved image processing techniques for optic disc segmentation in retinal fundus images, Biomed. Signal Process Control 58 (2020), 101832, <https://doi.org/10.1016/j.bspc.2019.101832>.
- [35] T.M. Khan, M. Mehmood, S.S. Naqvi, M.F.U. Butt, A region growing and local adaptive thresholding-based optic disc detection, PLoS One 15 (1) (2020), e0227566, <https://doi.org/10.1371/journal.pone.0227566>.
- [36] K.S. Nija, C.P. Anupama, V.P. Gopi, V.S. Anitha, Automated segmentation of optic disc using statistical region merging and morphological operations, Phys. Eng. Sci. Med. 43 (3) (2020) 857–869, <https://doi.org/10.1007/s13246-020-00883-2>.
- [37] R. Shanthi, S. Prabakaran, A review paper on an automatic localization of optic disc and segmentation approaches for glaucoma diagnosis, Int. J. Appl. Eng. Res. 10 (75) (2015) 2015.
- [38] M.N. Reza, Automatic detection of optic disc in color fundus retinal images using circle operator, Biomed. Signal Process Control 45 (2018) 274–283, <https://doi.org/10.1016/j.bspc.2018.05.027>.
- [39] A. Ali, W.M.D.W. Zaki, A. Hussain, N. Hashim, W.N.M. Isa, Vessel masking and Hough transform for optic disc localisation from retinal images, F1000Research 11 (181) (2022) 181, <https://doi.org/10.12688/f1000research.73390.1>.
- [40] J. Yi, Y. Ran, G. Yang, Particle swarm optimization-based approach for optic disc segmentation, Entropy 24 (6) (2022) 796, <https://doi.org/10.3390/e24060796>.
- [41] G.Y. Kim, S.H. Lee, S.M. Kim, Automated segmentation and quantitative analysis of optic disc and fovea in fundus images, Multimed. Tool. Appl. (2021) 1–16, <https://doi.org/10.1007/s11042-021-10815-1>.
- [42] Y. Kaya, A novel method for optic disc detection in retinal images using the cuckoo search algorithm and structural similarity index, Multimed. Tool. Appl. 79 (31) (2020) 23387–23400, <https://doi.org/10.1007/s11042-020-09080-5>.
- [43] A.S. Abdullah, Y.E. Özok, J. Rahebi, A novel method for retinal optic disc detection using bat meta-heuristic algorithm, Med. Biol. Eng. Comput. 56 (11) (2018) 2015–2024, <https://doi.org/10.1007/s11517-018-1840-1>.
- [44] N.F.A. Al Shalchi, J. Rahebi, Human retinal optic disc detection with grasshopper optimization algorithm, Multimed. Tool. Appl. (2022) 1–19, <https://doi.org/10.1007/s11042-022-12838-8>.
- [45] B.V. Kumar, S. Zhang, T. Wu, J. Prakash, L. Zhou, K. Li, A novel JAYA algorithm for optic disc localisation in eye fundus images, Int. J. Comput. Vis. Robot 12 (3) (2022) 324–342, <https://doi.org/10.1504/IJCVR.2022.10044827>.
- [46] R. Xu, D. Wunsch, Survey of clustering algorithms, IEEE Trans. Neural Network. 16 (3) (2005) 645–678.
- [47] M. Abdullah, M.M. Fraz, S.A. Barman, Localization and segmentation of optic disc in retinal images using circular Hough transform and grow-cut algorithm, PeerJ 4 (2016), e2003, <https://doi.org/10.7717/peerj.2003>.
- [48] B. Al-Bander, B.M. Williams, W. Al-Nuaimy, M.A. Al-Taee, H. Pratt, Y. Zheng, Dense fully convolutional segmentation of the optic disc and cup in colour fundus for glaucoma diagnosis, Symmetry 10 (4) (2018) 87, <https://doi.org/10.3390/sym10040087>.
- [49] A. Diaz-Pinto, S. Morales, V. Naranjo, T. Köhler, J.M. Mossi, A. Navea, CNNs for automatic glaucoma assessment using fundus images: an extensive validation, Biomed. Eng. Online 18 (1) (2019) 1–19, <https://doi.org/10.1186/s12938-019-0649-y>.
- [50] A. Joshi, K.K. Sharma, Graph deep network for optic disc and optic cup segmentation for glaucoma disease using retinal imaging, Phys. Eng. Sci. Med. (2022) 1–12, <https://doi.org/10.1007/s13246-022-01154-y>.
- [51] J. Latif, S. Tu, C. Xiao, S. Ur Rehman, A. Imran, Y. Latif, ODGNet: a deep learning model for automated optic disc localization and glaucoma classification using fundus images, SN Appl. Sci. 4 (4) (2022) 1–11, <https://doi.org/10.1007/s42452-022-04984-3>.
- [52] O. Saha, R. Sathish, D. Sheet, Learning with multitask adversaries using weakly labelled data for semantic segmentation in retinal images, in: International Conference on Medical Imaging with Deep Learning, PMLR, 2019, May, pp. 414–426.
- [53] L. Yu, Joint segmentation of optic cup and optic disc using deep convolutional generative adversarial network, in: Journal of Physics: Conference Series, vol. 2234, IOP Publishing, 2022, April, 012008.
- [54] T.H. Carvalho, C.H. Moraes, R.C. Almeida, D.H. Spadoti, Application of conditional GAN models in optic disc/optic cup segmentation of retinal fundus images, in: 17th International Symposium on Medical Information Processing and Analysis, vol. 12088, SPIE, 2021, December, pp. 389–395.
- [55] A.S. Hervella, J. Rouco, J. Novo, M. Ortega, End-to-end multi-task learning for simultaneous optic disc and cup segmentation and glaucoma classification in eye fundus images, Appl. Soft Comput. 116 (2022), 108347.
- [56] H. Xiong, S. Liu, R.V. Sharai, E. Coiera, S. Berkovsky, Weak label based Bayesian U-Net for optic disc segmentation in fundus images, Artif. Intell. Med. 126 (2022), 102261, <https://doi.org/10.1016/j.artmed.2022.102261>.
- [57] L. Wang, H. Liu, Y. Lu, H. Chen, J. Zhang, J. Pu, A coarse-to-fine deep learning framework for optic disc segmentation in fundus images, Biomed. Signal Process Control 51 (2019) 82–89, <https://doi.org/10.1016/j.bspc.2019.01.022>.
- [58] Z. Gu, J. Cheng, H. Fu, K. Zhou, H. Hao, Y. Zhao, J. Liu, Ce-net: context encoder network for 2d medical image segmentation, IEEE Trans. Med. Imag. 38 (10) (2019) 2281–2292, <https://doi.org/10.1109/TMI.2019.2903562>.
- [59] M. Tabassum, T.M. Khan, M. Arsalan, S.S. Naqvi, M. Ahmed, H.A. Madni, J. Mirza, CDED-Net: joint segmentation of optic disc and optic cup for glaucoma screening, IEEE Access 8 (2020) 102733–102747, <https://doi.org/10.1109/ACCESS.2020.2998635>.
- [60] Z. Lu, D. Chen, Weakly supervised and semi-supervised semantic segmentation for optic disc of fundus image, Symmetry 12 (1) (2020) 145, <https://doi.org/10.3390/sym12010145>.
- [61] M.K. Hasan, M.A. Alam, M.T.E. Elahi, S. Roy, R. Martí, DRNet: segmentation and localization of optic disc and Fovea from diabetic retinopathy image, Artif. Intell. Med. 111 (2021), 102001, <https://doi.org/10.1016/j.artmed.2020.102001>.
- [62] C. Shi, J. Zhang, X. Zhang, M. Shen, H. Chen, L. Wang, A recurrent skip deep learning network for accurate image segmentation, Biomed. Signal Process Control 74 (2022), 103533, <https://doi.org/10.1016/j.bspc.2022.103533>.
- [63] T.T. Khaing, T. Ruenmark, P. Aimanee, S. Makhanov, N. Kanchanaranya, Glaucoma detection in mobile phone retinal images based on ADI-GVF segmentation with EM initialization, ECTI Trans. Comput. Inf. Technol. (ECTI-CIT) 15 (1) (2021) 134–149, <https://doi.org/10.37936/ecti-cit.2021151.227261>.
- [64] J. Escorcia-Gutierrez, J. Torrents-Barrena, M. Gamarra, P. Romero-Aroca, A. Valls, D. Puig, A color fusion model based on Markowitz portfolio optimization for optic disc segmentation in retinal images, Expert Syst. Appl. 174 (2021), 114697, <https://doi.org/10.1016/j.eswa.2021.114697>.
- [65] X. Zhao, S. Wang, J. Zhao, H. Wei, M. Xiao, N. Ta, Application of an attention U-Net incorporating transfer learning for optic disc and cup segmentation, Signal Image Video Process. 15 (5) (2021) 913–921, <https://doi.org/10.1007/s11760-020-01815-z>.
- [66] Y. Zhang, X. Cai, Y. Zhang, H. Kang, X. Ji, X. Yuan, TAU: transferable Attention U-Net for optic disc and cup segmentation, Knowl. Base Syst. 213 (2021), 106668, <https://doi.org/10.1016/j.knosys.2020.106668>.
- [67] W. Zhou, S. Qiao, Y. Yi, N. Han, Y. Chen, G. Lei, Automatic optic disc detection using low-rank representation based semi-supervised extreme learning machine, Int. J. Mach. Learn. Cybern. 11 (1) (2020) 55–69, <https://doi.org/10.1007/s13042-019-00939-0>.
- [68] Y. Wang, X. Yu, C. Wu, Optic disc detection based on fully convolutional neural network and structured matrix decomposition, Multimed. Tool. Appl. 81 (8) (2022) 10797–10817, <https://doi.org/10.1007/s11042-022-12235-1>.
- [69] Y. Huang, Z. Zhong, J. Yuan, X. Tang, Efficient and robust optic disc detection and fovea localization using region proposal network and cascaded network, Biomed. Signal Process Control 60 (2020), 101939, <https://doi.org/10.1016/j.bspc.2020.101939>.
- [70] L.K. Singh, H. Garg, Automated glaucoma type identification using machine learning or deep learning techniques, in: Advancement of Machine Intelligence in Interactive Medical Image Analysis, Springer, Singapore, 2020, pp. 241–263, https://doi.org/10.1007/978-981-15-1100-4_12.
- [71] L.K. Singh, H. Garg, M. Khanna, Deep learning system applicability for rapid glaucoma prediction from fundus images across various data sets, Evol. Syst. (2022) 1–30, <https://doi.org/10.1007/s12530-022-09426-4>.
- [72] L.K. Singh, Pooja, H. Garg, et al., An enhanced deep image model for glaucoma diagnosis using feature-based detection in retinal fundus, Med. Biol. Eng. Comput. 59 (2021) 333–353, <https://doi.org/10.1007/s11517-020-02307-5>.
- [73] R.N. Johnson, A.D. Fu, H.R. McDonald, J.M. Jumper, E. Ai, E.T. Cunningham, B. J. Lujan, Fluorescein Angiography: Basic Principles and Interpretation, retina fifth ed., Elsevier Inc, 2012, pp. 2–50, <https://doi.org/10.1016/B978-1-4557-0737-9.00001-1>.
- [74] K. He, J. Sun, X. Tang, Single image haze removal using dark channel prior, IEEE Trans. Pattern Anal. Mach. Intell. 33 (12) (2010) 2341–2353, <https://doi.org/10.1109/CVPR.2009.5206515>.
- [75] K. Zuiderveld, Contrast limited adaptive histogram equalization, Graphics Gems (1994) 474–485, <https://doi.org/10.1109/ICACCI.2014.6968381>.
- [76] J. Bernsen, Dynamic thresholding of gray-level images, in: Proc. Eighth Int'l Conf. Pattern Recognition, Paris, 1986, 1986.
- [77] M.P. Sarathi, M.K. Dutta, A. Singh, C.M. Travieso, Blood vessel inpainting based technique for efficient localization and segmentation of optic disc in digital fundus images, Biomed. Signal Process Control 25 (2016) 108–117, <https://doi.org/10.1016/j.bspc.2015.10.012>.
- [78] R.C. Gonzalez, R.E. Woods, B.R. Masters, Digital Image Processing, 2009.

- [79] L. Vincent, Morphological grayscale reconstruction in image analysis: applications and efficient algorithms, *IEEE Trans. Image Process.* 2 (2) (1993) 176–201, <https://doi.org/10.1109/83.217222>.
- [80] J. Sivaswamy, S.R. Krishnadas, G.D. Joshi, M. Jain, A.U.S. Tabish, Drishti-gs: retinal image dataset for optic nerve head (ohn) segmentation, in: 2014 IEEE 11th International Symposium on Biomedical Imaging (ISBI), IEEE, 2014, April, pp. 53–56, <https://doi.org/10.1109/ISBI.2014.6867807>.
- [81] H. Yu, E.S. Barriga, C. Agurto, S. Echegaray, M.S. Pattichis, W. Bauman, P. Soliz, Fast localization and segmentation of optic disk in retinal images using directional matched filtering and level sets, *IEEE Trans. Inf. Technol. Biomed.* 16 (4) (2012) 644–657, <https://doi.org/10.1109/TITB.2012.2198668>.
- [82] H.A. Quigley, A.E. Brown, J.D. Morrison, S.M. Drance, The size and shape of the optic disc in normal human eyes, *Arch. Ophthalmol.* 108 (1) (1990) 51–57, <https://doi.org/10.1001/archoph.1990.01070030057028>.
- [83] X. Yao, D. Toslak, T. Son, J. Ma, Understanding the relationship between visual-angle and eye-angle for reliable determination of the field-of-view in ultra-wide field fundus photography, arXiv preprint arXiv:2106.09095, <https://doi.org/10.1364/BOE.433775>, 2021.
- [84] D.A. Dharmawan, B.P. Ng, S. Rahardja, A new optic disc segmentation method using a modified Dolph-Chebyshev matched filter, *Biomed. Signal Process Control* 59 (2020), 101932, <https://doi.org/10.1016/j.bspc.2020.101932>.
- [85] R. Romero-Oraá, J. Jiménez-García, M. García, M.I. López-Gálvez, J. Oraá-Pérez, R. Hornero, Entropy rate superpixel classification for automatic red lesion detection in fundus images, *Entropy* 21 (4) (2019) 417, <https://doi.org/10.3390/e21040417>.
- [86] C.G. Owen, A.R. Rudnicka, R. Mullen, S.A. Barman, D. Monekosso, P.H. Whincup, C. Paterson, Measuring retinal vessel tortuosity in 10-year-old children: validation of the computer-assisted image analysis of the retina (CAIAR) program, *Invest. Ophthalmol. Vis. Sci.* 50 (5) (2009) 2004–2010, <https://doi.org/10.1167/iovs.08-3018>.
- [87] J. Staal, M.D. Abràmoff, M. Niemeijer, M.A. Viergever, B. Van Ginneken, Ridge-based vessel segmentation in color images of the retina, *IEEE Trans. Med. Imag.* 23 (4) (2004) 501–509, <https://doi.org/10.1109/TMI.2004.825627>.
- [88] A. Budai, R. Bock, A. Maier, J. Hornegger, G. Michelson, Robust vessel segmentation in fundus images, *Int. J. Biomed. Imag.* (2013), <https://doi.org/10.1155/2013/154860>, 2013.
- [89] J. Sivaswamy, S. Krishnadas, A. Chakravarty, G. Joshi, A.S. Tabish, A comprehensive retinal image dataset for the assessment of glaucoma from the optic nerve head analysis, *JSM Biomed. Imag. Data Pap.* 2 (1) (2015) 1004, <https://doi.org/10.1109/JISBL.2014.6867807>.
- [90] E.J. Carmona, M. Rincón, J. García-Feijoó, J.M. Martínez-de-la-Casa, Identification of the optic nerve head with genetic algorithms, *Artif. Intell. Med.* 43 (3) (2008) 243–259, <https://doi.org/10.1016/j.artmed.2008.04.005>.
- [91] F. Fumero, S. Alayón, J.L. Sanchez, J. Sigut, M. Gonzalez-Hernandez, RIM-ONE: an open retinal image database for optic nerve evaluation, in: 2011 24th International Symposium on Computer-Based Medical Systems (CBMS), IEEE, 2011, June, pp. 1–6, <https://doi.org/10.1109/CBMS.2011.5999143>.
- [92] P. Porwal, S. Pachade, R. Kamble, M. Kokare, G. Deshmukh, V. Sahasrabuddhe, F. Meriaudeau, Indian diabetic retinopathy image dataset (IDRiD): a database for diabetic retinopathy screening research, *Data* 3 (3) (2018) 25, <https://doi.org/10.21227/H25W98>.
- [93] A. Almazroa, S. Alodhayb, E. Osman, E. Ramadan, M. Hummadi, M. Dlaim, V. Lakshminarayanan, Retinal fundus images for glaucoma analysis: the RIGA dataset, in: Medical Imaging 2018: Imaging Informatics for Healthcare, Research, and Applications, vol. 10579, International Society for Optics and Photonics, 2018, March, p. 105790B, <https://doi.org/10.1117/12.2293584>.